Journal of
Medicinal Chemistry



Article

# Discovery of novel peptidomimetic boronate ClpP inhibitors with noncanonical enzyme mechanism as potent virulence blockers in vitro and in vivo

Yuan Ju, Lihui He, Yuanzheng Zhou, Tao Yang, Ke Sun, Rao Song, Yang Yang, Chengwei Li, Zitai Sang, rui bao, and Youfu Luo

*J. Med. Chem.*, **Just Accepted Manuscript** • DOI: 10.1021/acs.jmedchem.9b01746 • Publication Date (Web): 07 Feb 2020



## Just Accepted



is published by the American Chemical Society. 1155 Sixteenth Street N.W., Washington, DC 20036

# Discovery of novel peptidomimetic boronate ClpP inhibitors with noncanonical enzyme mechanism as potent virulence blockers *in vitro* and *in vivo*

*Yuan Ju,*[#,a] *Lihui He,*[#,a] *Yuanzheng Zhou,*[#,a] *Tao Yang*[#,a,b] *Ke Sun,*[a] *Rao Song,*[a] *Yang Yang,*[a] *Chengwei Li,*[a,c] *Zitai Sang,*[d] *Rui Bao**[a] *and Youfu Luo**[a]

[a]State Key Laboratory of Biotherapy and Cancer/Collaborative Innovation Center for Biotherapy, West China Hospital, Sichuan University, Chengdu 610041, China

[b]Laboratory of Human Disease and Immunotherapies, West China Hospital, Sichuan University, Chengdu 610041, China

[c]Suzhou Zelgen Biopharmaceuticals Co., Ltd., Kunshan, Jiangsu 215301, China

[d]Institute of Life Science, Luoyang Normal University, Luoyang, Henan 471934, China

*Corresponding authors. Email: luo_youfu@scu.edu.cn, baorui@scu.edu.cn

[#]These authors contributed equally to this work.

**Abstract**

Caseinolytic protease P (ClpP) is considered as a promising target for the treatment of *Staphylococcus aureus* infections. In an unbiased screen of 2632 molecules, a peptidomimetic boronate, MLN9708, was found to be a potent suppressor of *Sa*ClpP function. A time-saving and cost-efficient strategy integrating *in silico* position scanning, multistep miniaturized synthesis, and bioactivity testing was deployed for optimization of this hit compound and led to fast exploration of structure-activity relationships. Five of 150 compounds from the miniaturized synthesis exhibited improved inhibitory activity. Compound **43Hf** was the most active inhibitor and showed reversible covalent binding to *Sa*ClpP while did not destabilize the tetradecameric structure of *Sa*ClpP. The crystal structure of **43Hf**-*Sa*ClpP complex provided mechanistic insight into the covalent binding mode of peptidomimetic boronate and *Sa*ClpP. Furthermore, **43Hf** could bind endogenous ClpP in *S. aureus* cells, and exhibited significant efficacy in attenuating *S. aureus* virulence *in vitro* and *in vivo*.

## Introduction

The caseinolytic protease proteolytic subunit (ClpP) is a highly conserved serine protease that plays an essential role in bacterial cell homeostasis by degrading damaged and short-lived regulatory proteins. Alteration of ClpP activity is associated with diverse biological functions in many pathogenic bacteria.[1] In Actinomycetales such as *Mycobacterium tuberculosis* and *Corynebacterium glutamicum*, ClpP was found to be essential for bacterial viability.[2] In *Staphylococcus aureus*,[3] *Listeria monocytogenes*,[4] *Streptococcus pneumoniae*,[5] and *Pseudomonas aeruginosa*,[6] even though ClpP is not essential for bacterial survival, it is vital for their pathogenicity. Thus, as widespread bacterial resistance to antibiotics making the treatment of infectious diseases more challenging, chemically targeting ClpP has been recognized as a promising anti-virulence strategy. Such a strategy would combat pathogenesis with less evolutionary pressure towards drug resistance, and limit the detrimental impact of antibiotics on the host microbiome.[7]

*S. aureus* is a major human pathogen that causes a variety of infections including scalded skin syndrome, sepsis and meningitis.[8] *S. aureus* ClpP (*Sa*ClpP) was found to have a profound influence on the secretion of α-hemolysin (Hla) by regulating factors encoded by the accessory gene regulator (agr) locus, such as RNAIII transcript.[9] Genetic clpP knockout in S. aureus attenuated virulence in a murine skin abscess model,[3] and a similar phenotype was observed upon inhibition of *Sa*ClpP with β-lactones, the first-generation ClpP inhibitor.[10] β-Lactones can covalently acylate the catalytic serine residue of ClpP; a derivative compound, D3, lead to obvious

elimination of the extracellular virulence of *S. aureus* at nanomolar concentration.[10,11] However, the β-lactones are unstable and quickly hydrolyzed in human plasma.[10] In addition, compound AV170, a phenol ester, can covalently modify the active site of *Sa*ClpP and depolymerize the tetradecameric proteolytic enzyme complex into inactive heptamers. However, AV170 is not suitable for further in vivo investigation due to the instability of phenol ester bond.[12] The first non-covalent oxazole inhibitor of *Sa*ClpP, AV145, can bind to the handle region close to the active site; however, the chaperone ClpX revoked the inhibitory effect.[13] Novel inhibitors of ClpP from other species are also under development. Boron-based peptidomimetics, including bortezomib (BTZ) and substrate-like peptide boronate inhibitors, have been shown to be potent covalent inhibitors of *Mt*ClpP1P2 from *M. tuberculosis* and *h*ClpXP from human.[14-16] In addition, pyrimidines have been shown to inhibit PfClpP from *Plasmodium falciparum*.[17] The chloromethyl ketone Z-LY-CMK and α-amino diphenyl phosphonates have been identified as inhibitors of *Ec*ClpP from *Escherichia coli*, but some of these inhibitors lacked the efficacy in the nitric oxide stress assay.[18,19] Nevertheless, the chemical structure types of *Sa*ClpP inhibitors are rather quite limited. To expand the arsenal of ClpP inhibitors and further improve their pharmacological application, there is a pressing need to develop novel compounds with stable scaffolds and promising anti-virulence activity both in vitro and in vivo.

The traditional design–synthesis–purification–assay workflow is still widely used in drug candidate discovery. However, the hazardous and time-consuming process, which takes 1–8 weeks for every cycle and involves relatively high consumption of

chemical materials, limits the use of these techniques on a larger scale.[20] For bioassays that can couple with miniaturized chemical synthesis approaches, including one-bead one-compound libraries,[21] DNA-encoding chemical libraries,[22] mass-encoding technology, dynamic combinatorial chemistry,[23] and nanoscale synthesis with affinity ranking,[24] the integration of synthesis and assay could greatly reduce the material requirements and enable rapid analysis. Most such approaches depend on delicate purification during the process of library synthesis, and integration of miniaturized synthesis and testing without complicated workup has been predominantly applied in one-step reactions. It remains challenging to use this strategy for compounds requiring multistep synthesis.

In this study, considering that *in silico* structure-based activity predication can significantly accelerate the hit to lead process,[25] we used an integrated strategy cascading *in silico* position scanning, multistep synthesis, and peptidase inhibition activity testing to improve the inhibitory effect against *Sa*ClpP of our initial hit compound MLN9708 (randomly screened from 2632 compounds). The integrated strategy rationally and rapidly generated syntheses with high diversity at each position. Notably, each reaction was performed at 0.1 M concentration in separated microplate wells with minimum material consumption, the direct bioassay of crude products also avoids the lengthy workup steps. Next, we performed scaled-up synthesis of the promising products and tested their effect on virulence of *S. aureus* both in vitro and in vivo. The most active compound, **43Hf**, was co-crystallized with *Sa*ClpP, and the detailed binding mode was elucidated. Compound **43Hf** showed reversible covalent

binding with the active site serine residue of *Sa*ClpP while the protein maintained its tetradecameric assembly.

## Results

### Identification of the peptidomimetic boronate MLN 9708 as an *Sa*ClpP inhibitor

To identify hit compounds targeting *Sa*ClpP, we performed a random screen using an in-house library of 2632 bioactive chemicals (Fig. 1a). In the primary screen, compounds were assayed at a single-point concentration of 10 μM and eight initial hits (hit rate 0.3 %) were selected based on their >50% inhibitory effects on *Sa*ClpP cleavage activity towards substrate Suc-LY-AMC (Figs. 1a, 2a and 2b). In the secondary screen, initial hits were evaluated in a concentration-dependent manner and five hits with low $IC_{50}$ values were selected for further studies (Figs. 1a and 2c). Differential scanning calorimetry analysis showed that, among the five hits, compound F significantly shifted melting peak of *Sa*ClpP (from 50.8 °C to 77.5 °C) and the $EC_{50}$ value was 19.90 ± 1.17 μM, indicating direct binding (Fig. 2d). Moreover, compound F also stood out in the substrate competition assay (Fig. 2e), in which the increased substrate concentration had minimal influence on its inhibitory activity.

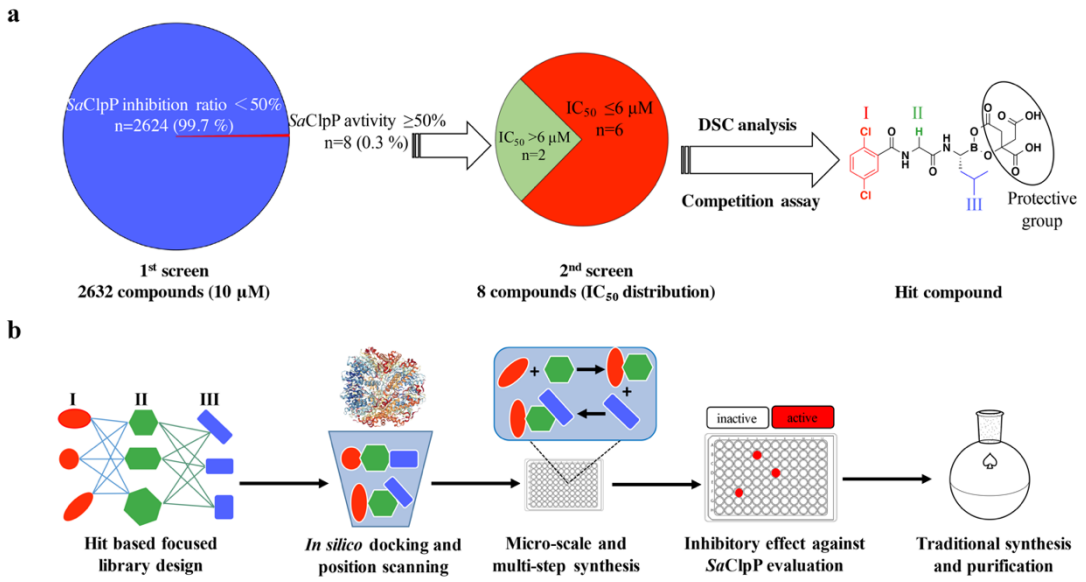


**Figure 1.** Schematic illustration of chemical screening and structural optimization process. (a) Identification of novel *Sa*ClpP inhibitor hits in an in-house library containing 2632 bioactive small-molecule compounds. (b) Cartoon depicting the integrated strategy to the optimize hit compound MLN9708.

The hit compound F is ixazomib citrate (MLN9708), which can be immediately hydrolyzed to its biologically active form ixazomib (MLN2238) (Fig. 1a).[26] The dissociation constant ($K_d$) for MLN9708 binding to *Sa*ClpP is about 7.3 ± 1.1 μM according to the isothermal titration calorimetry (ITC) assay (Fig. S1). The active form MLN2238 has a similar structure to that of the *Mt*ClpP1 inhibitor BTZ, which also showed efficient inhibition of *Sa*ClpP ($IC_{50}$ value of 5.3 ± 0.2 μM) (Fig. 2b; Table 1),[14] indicating that they may share a common mechanism of ClpP inhibition. Boron-based peptidomimetic molecules have been recognized to be potent inhibitors of proteases;[27] because the boronate warhead is a strong electrophile and behaves as a Lewis acid, it is capable of forming dative bonds with nucleophilic residues like

serine or threonine, resulting in an anionic tetragonal structure.[28,29] In *Sa*ClpP, the active-site residue Ser98 is the most probable site for boronate binding, while the inhibitory potency can be improved by optimizing the other moieties of the boronate inhibitor.

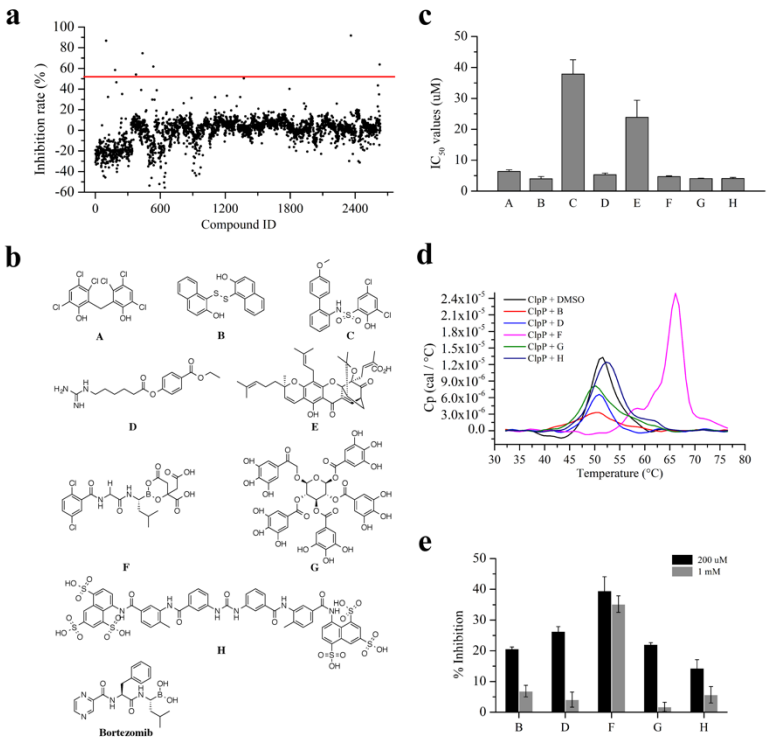


**Figure 2.** Discovery of a novel *Sa*ClpP inhibitor MLN9708 from the chemical library screen. (a) A random screen of 2362 compounds identified eight primary hits with >50% inhibitory effect at 10 μM. Each circle represents the mean percentage inhibition for a compound tested at 10 μM in triplicate. (b) Structures of the eight initial hits and bortezomib (BTZ). (c) $IC_{50}$ values of compounds A–H toward *Sa*ClpP. (d) Thermal shift assays of the binding between five hits (at 100 μM) and *Sa*ClpP. (e) Inhibition of *Sa*ClpP peptidase activity by 3 μM compounds B, D, F, G and H in the presence of 200 μM or 1 mM Suc-LY-AMC substrate. The error bars of panels (c) and (e) represent the SD in three independent replicate determinations.

**Optimization of MLN9708/BTZ through the integrated strategy**

The integrated strategy—including computational ranking, multistep microscale synthesis, and cascaded biological testing—is illustrated in Figure 1b. The *in silico* step involved virtual focused library construction and position scanning. A virtual focused library containing the boronate warhead was automatically constructed by substituent random combinations. To conduct the *in silico* position scanning, 17 libraries (libraries A–Q), which had different amino acids for II moiety (Figs. 3a and S2), were generated. Each library contained 258 individual chemicals, including 43 carboxylic acids as building blocks for moiety I, and 6 boronate building blocks for moiety III (Fig. S2). Docking of the ligands into the active site of *Sa*ClpP was performed with the Schrödinger suite and the best pose of each molecule was ranked according to the GlideScore. A heat map of the docking scores showed significant differentiation at each position (Fig. 3a). Molecules with a score lower than that of MLN2238 (−6.24 kcal/mol) were selected and the frequency of occurrence of each group was counted: only seven fragments occurred <40 times in the I position, while nine II fragments and all the III fragments occurred >100 times (Fig. S3). Eventually, 30 commercially available building blocks for the I substituent, 5 for the II substituent, and 1 for the III substituent were selected for the next multistep miniaturized synthesis experiments (Figs. 4 and S2).

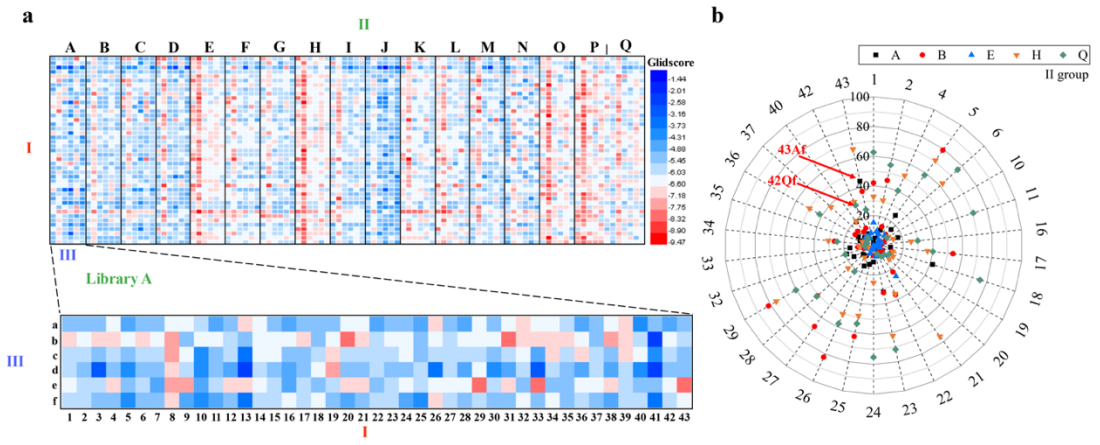


**Figure. 3** Ranking of the virtual focused library and activity of product mixtures derived from the micro-scale synthesis. (a) Heat map of the GlideScores of small molecules in virtual libraries A–Q. (b) Radial graph showing inhibitory effects of crude products obtained in micro-scale synthesis. The outer edge of the wheel represents 100% inhibition of *Sa*ClpP peptidase activity, while the center of the circle represents 0% inhibition. The numbers around the ring represent the group on moiety I, while the colors of the symbols represent the groups on moiety II. Each point represents the mean percentage inhibition for the mixture tested at Σ[Pn]=10 μM in triplicates.

To enable rapid and cost-efficient preparation of an extensive series of boronate warhead compounds, we used a micro-scale and multi-step synthetic system that could perform up to 96 reactions in parallel. In a proof of concept experiment, BTZ was used as the synthesis template to verify the efficiency of the miniaturized synthesis route (Fig. S4a). The multistep synthesis procedures were developed in microplates, followed by straightforward solvent extraction and evaporation. In this experiment, the ester product S1 (Fig. S4a) was obtained by coupling of

2-pyrazinecarboxylic acid and methyl L-phenylalaninate, then, the ester was hydrolyzed in basic conditions to furnish carboxylic acids product S2 (Fig. S4a). Product S3 (*N*-((*S*)-1-(((*R*)-3-methyl-1-((3a*S*,4*S*,6*S*,7a*R*)-3a,5,5-trimethylhexahydro-4,6-methanobenzo[*d*][1,3,2]dioxaborol-2-yl)butyl)amino)-1-oxo-3-phenylpropan-2--yl)pyrazine-2- carboxamide) was achieved by coupling (R)-BoroLeu-(+)-Pinanediol trifluoroacetate with S2, and was subsequently deprotected to provide the target boronate compound S4 (Fig. S4a). High-performance liquid chromatography (HPLC) analysis indicated that BTZ was present in the crude product and the final yield was about 28% (Fig. S4b). To be noted, none of the intermediate products demonstrated inhibitory activity towards *Sa*ClpP (Fig. S5). Taken together, we concluded that it is feasible to synthesize boronate warhead inhibitors in a micro-scale and multistep system, and the resultant library members can be assayed directly without the need for delicate purification procedures.

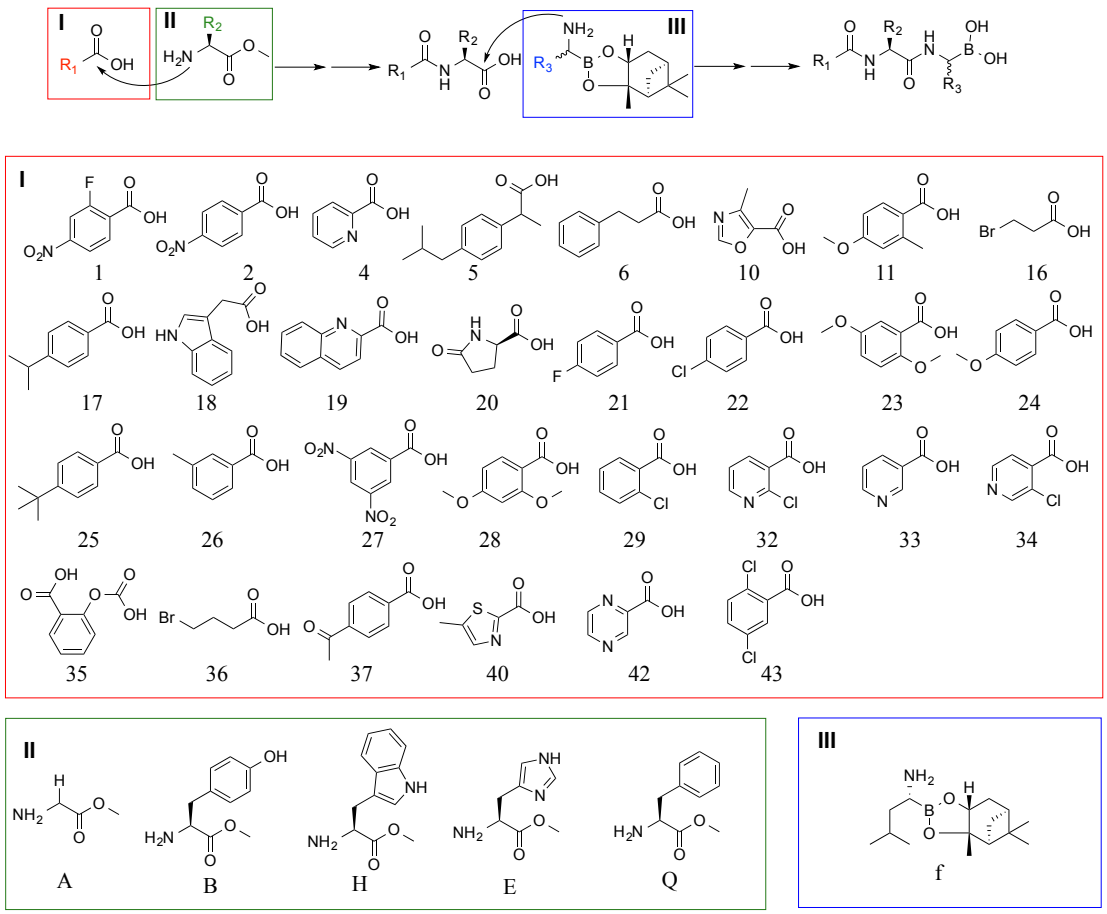


**Figure 4.** Synthetic strategy and building blocks for moieties I, II and III for the combinatorial synthesis of a 150-member library of the boronate peptidomimetics.

To efficiently and rapidly explore the preliminary structure–activity relationship (SAR) of the boronate peptidomimetics toward *Sa*ClpP, we performed the micro-scale combinatorial synthesis and bioassay in 96-well plates. In parallel, MLN2238 (**43Af**) and BTZ (**42Qf**) were synthesized as controls. The multistep and micro-scale synthesis in individual wells allowed us to trace the products structure clearly (Figs. 1b and 4). In the first step, combinations of building blocks for moieties I and II were employed to give 150 (30 × 5) intermediates. Next, by coupling the intermediates with (R)-aminoboronate ester and deprotection, we totally obtained 150 target

boronate products (Fig. 4). Biological testing of the crude products as inhibitors of *Sa*ClpP was performed at a single-point concentration of 10 μM. Certain compounds that were better inhibitors than MLN2238 (**43Af**) or BTZ (**42Qf**) were selected to further determine their $IC_{50}$ values (Fig. 3b; Table S1). Note that the building blocks were all inactive towards *Sa*ClpP (Fig. S6). Five products with low $IC_{50}$ values were qualitatively analyzed by ultra-performance liquid chromatography–mass spectrometry (UPLC–MS) to confirm the formation of the correct chemicals. The contents of the expected molecules, which proved to be the main products in the crude products by UPLC–MS, was subsequently measured by HPLC and determined by area normalization method (Fig. S7). Then, scaled-up synthesis of these five inhibitors was performed in glassware vessels and they were purified by column chromatography (Scheme 1). The dose-dependent inhibition of *Sa*ClpP was determined (Table 1). The results validated the improved inhibitory activity of the products optimized by the miniaturized system ($IC_{50}$ values ranging from 0.9 μM to 1.9 μM) compared with 5.7 μM for MLN9708 and 5.3 μM for BTZ.

**Scheme 1.** Synthesis of compounds **5Bf**, **5Hf**, **43Hf**, **11Qf** and **24Qf**.

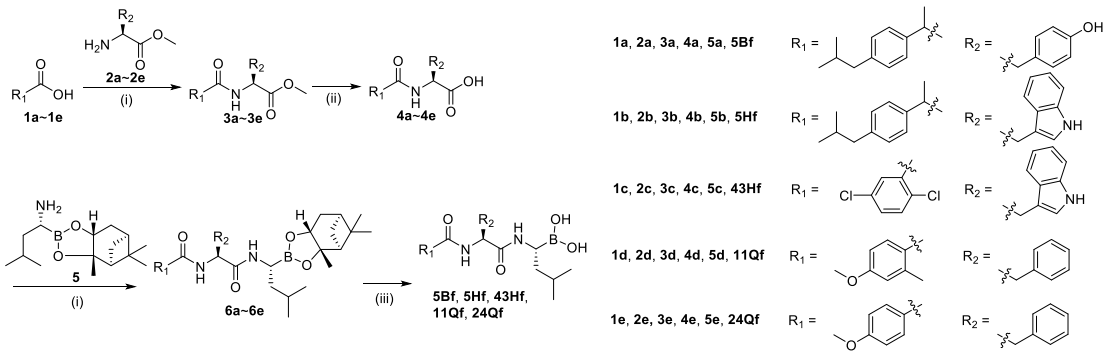


Reagents and conditions: (i) HATU, TEA, DCM, r.t., overnight; (ii) LiOH, $H_2O$/THF/MeOH, 0 °C, overnight; (iii) isobutaneboronic acid, aqueous HCl, EA/MeOH, r.t., overnight, yields: 15.1%–23.1%.

Thus, some preliminary SAR can be inferred from the micro-scale combinatorial screening. For discussion purposes, we divided these 150 crude products into five series (series A, B, E, H and Q) according to the different groups at the II position. Compounds of series A and E with hydrogen or *1H*-imidazole-4-methyl group at the II position exhibited weakened inhibition potency compared with MLN2238 or BTZ; none of these 60 compounds (30 in series A and 30 in series E) exhibited better inhibitory effects than MLN2238 at 10 μM (Fig. 3b). These data suggest that Gly and His may not be preferential amino acids as the building blocks for moiety II. Compounds of series B, H and Q yielded several *Sa*ClpP inhibitors that were more potent than MLN2238 (8 compounds in series B, 10 compounds in series H and 12 compounds in series Q). Among them, five compounds from series Q showed >70% inhibition at 10 μM (Fig. 3b), suggesting that groups with phenyl substituent may

perform better at position II. Considering moiety I, compounds with 1-(4-isobutylphenyl)ethan-1-yl or *m*-methylphenyl substituent from series B, compounds with 1-(4-isobutylphenyl)ethan-1-yl or 4-fluorophenyl substituent of series H, compounds with phenethyl, 2-methyl-4-methoxyphenyl, indole-3-methyl, 2,5-dimethoxyphenyl or 4-methoxyphenyl substituents from series Q showed >70% inhibition at 10 μM (Fig. 3b), suggesting that aromatic rings at position I may contribute to *Sa*ClpP inhibition. $IC_{50}$ values of compounds that showed greater inhibition than the hit controls were determined (Table S1). Compounds with 2,5-dichlorophenyl, 1-(4-isobutylphenyl)ethan-1-yl, *tert*-butylphenyl, *m*-methylphenyl, 3,5-dinitrophenyl, 2,4-dimetoxyphenyl, 2,5-dimetoxyphenyl, *p*-methoxyphenyl, *o*-chlorophenyl, pyridine-2-yl, 2-chloropyridine-4-yl, 2-methyl-4-metoxyphenyl or indole-3-methyl groups at position I exhibited greater inhibition potency ($IC_{50}$ < 10 μM) against *Sa*ClpP than those with other substituents at this position. Taken together, we conclude that aromatic groups with phenyl group at position II and aromatic rings with electron-donating groups at position I were more beneficial for inhibition of *Sa*ClpP.

**Table 1.** Peptidase inhibitory activity, anti-virulence activity, hemolytic activity and cytotoxicity of the purified inhibitors.

| Entry | $IC_{50}$ [a] (μM) | $k_{inact}/K_i$ [b] ($10^2$/sM) | $EC_{50}$ [c] (μM) | $HC_{50}$ [d] (μM) | $GI_{50}$ [e] (μM) | |
|---|---|---|---|---|---|---|
| | | | | | HeLa | HepG2 |
| MLN | 5.7 ± 0.01 | 2.4 ± 0.07 | 3.6 ± 0.2 | 408 | 181.8 ± 2.1 | >200 |
| BTZ | 5.3 ± 0.2 | 2.2 ±0.1 | 23.5 ± 0.6 | >500 | 168.1 ± 1.7 | 100.6 ± 2.5 |
| 5Bf | 1.4 ± 0.1 | 7.2 ± 0.3 | 9.6 ± 0.5 | >500 | 83.0 ± 2.1 | 116.8 ± 3.4 |
| 5Hf | 1.9 ± 0.3 | 8.0 ± 1.0 | 2.6 ± 0.4 | >500 | 71.2 ± 2.2 | 54.8 ± 3.3 |
| 11Qf | 1.5 ± 0.2 | 9.1 ± 0.6 | 14.8 ± 0.9 | >500 | >200 | >200 |
| 24Qf | 1.9 ± 0.2 | 6.7 ± 0.7 | 3.3 ± 0.2 | >500 | 195.8 ± 1.9 | >200 |
| 43Hf | 0.9 ± 0.05 | 16.7 ± 0.2 | 1.4 ± 0.02 | >500 | 108.0 ± 3.1 | 83.4 ± 4.6 |

[a]Dose-dependent inhibition activity against *Sa*ClpP of the purified product. [b]Values determined from time-dependent $IC_{50}$ curves. [c]Determination of $EC_{50}$ values for hemolysis after treatment of MRSA with the inhibitors. [d]Hemolytic activity of inhibitors. [e] Values that inhibited the growth of the cells by 50%. The data represent the mean ± SD in three independent replicate determinations.

**Biochemical and biophysical characterization of the interaction between *Sa*ClpP and the optimized compounds**

Because of the time-dependent inhibition properties of covalent inhibitors, it is

suitable to further evaluate their activities by comparing the inhibition constant ($K_i$) and enzyme inactivation rate ($k_{inact}$).[30] $K_i$ and $k_{inact}$ values were calculated directly from the time-dependent $IC_{50}$ values as previously described.[31] Compared with the $k_{inact}/K_i$ values of MLN9708 ($2.4 \times 10^2$ /sM) and BTZ ($2.2 \times 10^2$ /sM), all of the optimized compounds showed approximately 3-fold to 7-fold higher $k_{inact}/K_i$ values, ranging from $6.7 \times 10^2$ /sM to $16.7 \times 10^2$ /sM (Table 1). This result confirmed that the optimization strategy had successfully improved the potency of the primary hits. Compound **43Hf** was verified as the most potent inhibitor.

To examine the direct interaction between the optimized inhibitors and *Sa*ClpP, thermal analysis was conducted by using differential scanning fluorimetry. All the optimized compounds exhibited enhanced abilities to progressively shift the transition midpoint of the heat denaturation curve by 29.5–42.2 °C comparing to the DMSO treated *Sa*ClpP (45.5 °C) (Fig. 5a). **43Hf** exerted the most significant effect ($\Delta T_m$ = +42.2 °C), with a half-maximal effective concentration of 1.27 μM (Figs. 5a and 5b), which confirmed that the affinity of **43Hf** for *Sa*ClpP was on the micromolar level. It worth noting that the reported covalent inhibitor AV170 barely impacted the thermal stability of *Sa*ClpP (Fig. 5a), indicating that the boronate peptidomimetics have a different inhibitory mechanism and distinct interaction pattern from that of AV170. This deduction was further supported by the size exclusion chromatography column and native-PAGE assays, in which the oligomeric states of *Sa*ClpP with or without boronate inhibitors were determined (Figs. 5c, 5d and S8). Distinct from the mechanism of compound AV170 which disrupted the ClpP tetradecamer into inactive

heptamers,[12] the boronates warhead inhibitors did not alter the tetradecameric assembly of *Sa*ClpP.

Next, we performed a dialysis experiment and measured the recovery rate of peptidase activity to test the reversibility of binding. The minimal changes in *Sa*ClpP inhibition by AV170 even after 72-h dialysis confirmed the permanent binding of this inhibitor to the protease active site (Fig. 5e). In contrast, for the boronate inhibitors, *Sa*ClpP activities were restored to nearly 100% after different periods of dialysis (Fig. 5e). The rates of recovery of activity were slower for the optimized compounds than for MLN9708 and BTZ. In particular, compounds with an indolyl group at the II position (**5Hf** and **43Hf**) showed the slowest recovery rates. These results suggest that the boronate inhibitors bound to *Sa*ClpP in a reversible, covalent fashion, and the indolyl group at position II might strengthen the binding. The reversible covalent inhibitory nature of the boronate compounds toward *Sa*ClpP would prevent the formation of permanent covalent adducts with off-target proteins, and it may be possible to optimize the inhibitor residence time at the active-site serine of *Sa*ClpP, which could facilitate the development of inhibitors with therapeutic applications.[33,34]

In *S. aureus* cells, *Sa*ClpP is in complex with *Sa*ClpX or *Sa*ClpC to execute the ATPase-dependent protein degradation function.[1] The *Sa*ClpXP activity can be determined *in vitro* by monitoring the degradation of fluorescein isothiocyanate-labeled casein (FITC-casein) substrate.[35] Using this approach, the optimized inhibitors were assayed for their inhibition of *Sa*ClpXP activity at concentrations of 100, 10 and 1 μM. In contrast to the initial hits BTZ and MLN9708,

which showed nearly no inhibition of *Sa*ClpXP, two of the optimized compounds were effective inhibitors; in particular, **43Hf** had an $IC_{50}$ value of 69.62 ± 2.94 μM (Fig. 5f). These results indicated that **43Hf** was also an efficient inhibitor of the *Sa*ClpXP complex.

Considering that the initial hit ixazomib is a marketed proteasome inhibitor and *Sa*ClpP is a serine protease, the target compounds were tested for their inhibitory effects on 20S proteasome, homologous PaClpP1 from *P. aeruginosa*,[36] hClpP[16] and other serine proteases, including HtrA-like serine protease AlgW[37] and trypsin-like serine protease Factor Xa (FXa).[38] The tested compounds **MLN9708**, **5Bf**, **43Hf** and **24Qf** inhibited 20S proteasome with nanomolar $IC_{50}$ values, and compound **43Hf** showed slightly lower activity than the others (Figure S9 and Table S2). All the tested analogues had slight selectivity for *Sa*ClpP against *h*ClpP and *Pa*ClpP1, with $IC_{50}$ between 3 to 25 μM for *h*ClpP and *Pa*ClpP1. Nevertheless, these boronate compounds showed little inhibition to AlgW and FXa at concentration up to 100 μM.

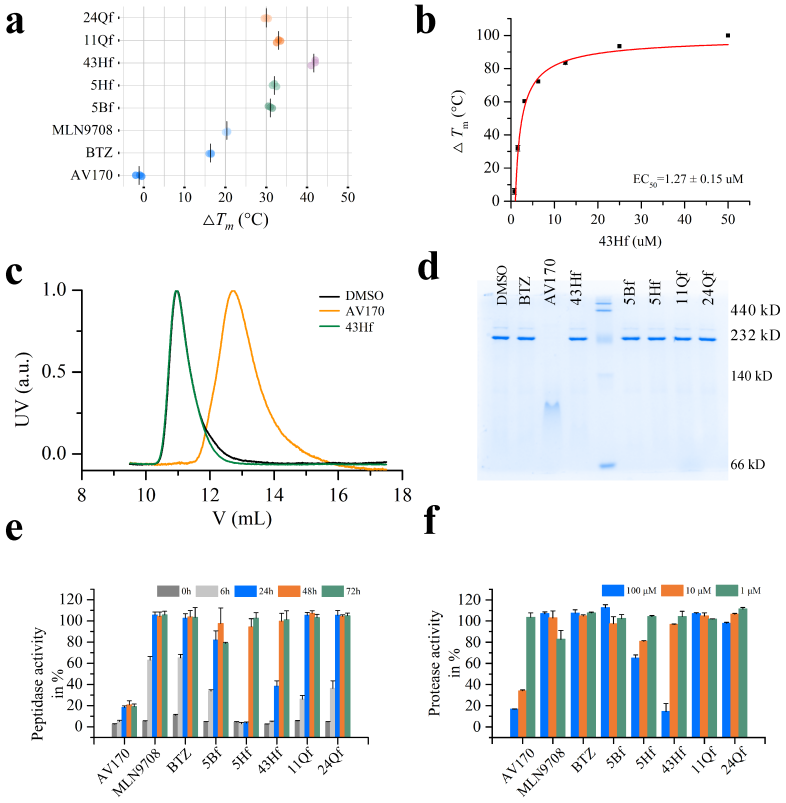


**Figure 5.** Inhibition potency and binding affinity of the optimized compounds. (a) Box plots representation of the direct interaction between the boronate compounds (50 μM) and *Sa*ClpP using differential scanning fluorimetry determination. Data were from three independent experiments, and the black lines represent the mean. (b) Strong stabilization of *Sa*ClpP folding by **43Hf** in a concentration-dependent manner. The data represent the mean ± SD in three independent replicate determinations. (c, d) Size-exclusion chromatograms and native-PAGE illustrating the retention of the tetradecameric state of *Sa*ClpP on treatment with the boronate compounds. (e) Peptidase activity recovery after dialysis of *Sa*ClpP pretreated with the inhibitor or DMSO. (f) Inhibition of *Sa*ClpXP protease activity by the inhibitors. The error bars of panels (e) and (f) represent the SD in three independent replicate determinations.

**Structural insights into the boronate inhibitor-bound *Sa*ClpP**

To determine the exact binding mode between the boronate compounds and *Sa*ClpP, BTZ and **43Hf** were respectively co-crystallized with *Sa*ClpP. The protein was prepared using similar expression and purification methods to those described previously.[12,39,40] The crystal structures were determined by molecular replacement using the *Sa*ClpP Y63A mutant structure (PDB code: 5C90) as the search model[39]. The final structure of **43Hf-**bound *Sa*ClpP was refined to 2.3Å resolution with $R_{work}$ of 19% and $R_{free}$ of 20%, and that of BTZ-bound *Sa*ClpP was refined to 2.2 Å resolution with $R_{work}$ of 24% and $R_{free}$ of 25% (Table S3). Like other reported ClpP structures,[13,16,39,41,42] *Sa*ClpP assembled into two heptameric rings that form a tetradecameric barrel. The inhibitors covalently bound to the active-site residue Ser98 in each subunit (Fig. 6). **43Hf**-bound *Sa*ClpP and BTZ-bound *Sa*ClpP were nearly identical in their overall structures, displaying a root mean square deviation (RMSD) value of 0.39Å for 1400 Cα atoms in tetradecamer–tetradecamer comparisons.

Despite variations in occupancy, model building into the averaged 2Fo−Fc electron-density map allowed the unambiguous positioning of **43Hf** (or BTZ) between helices α5 and α3 (Fig. 6b and 6c). Since the two boronates had similar binding patterns, we mainly focused on the **43Hf**-bound *Sa*ClpP structure in the following analysis. **43Hf** bound to the S1–S3 subsites of *Sa*ClpP and formed several hydrogen bonds with conserved residues, including Gly69, Ser70, Met99, His123 and Leu126 (Figs. 6b and 6d). The difference of hydrogen bond with Lue126 for **43Hf** comparing to BTZ interpreted the enhanced reversible covalent binding (Fig. 6d and

6e). A network of hydrophobic interaction contacts with Val71, Pro125, Gly127 and Ile143 further stabilized the compound binding. The boron atom of **43Hf** covalently interacted with the nucleophilic oxygen lone pair of Ser98O, while Gly69N and Met99N hydrogen-bridges to one of the acidic boronate hydroxyl groups. These boron atom-mediated interactions strengthened the anchoring in the active site oxyanion hole.

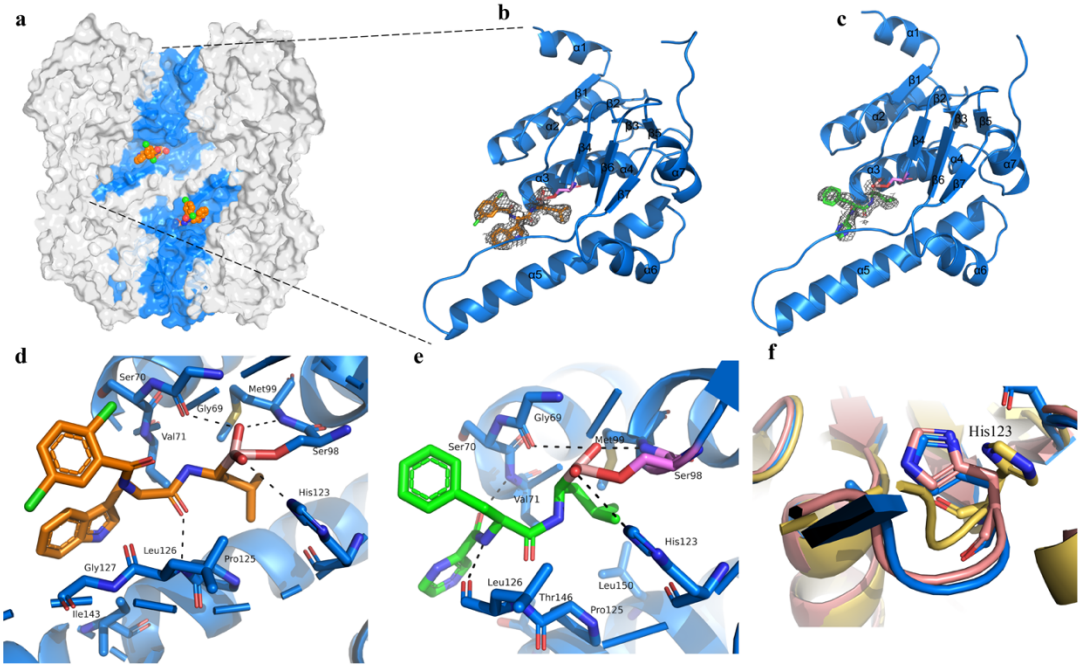


**Figure 6.** Co-crystal structure of *Sa*ClpP in complex with covalent inhibitor **43Hf** or BTZ. (a) Overall structures of **43Hf**-bound *Sa*ClpP. (b, c) Structural details of (b) **43Hf** and (c) BTZ binding pocket in *Sa*ClpP. The monomer *Sa*ClpP is shown as a blue cartoon, the inhibitors are shown as sticks. 2Fo−Fc electron-density maps of **43Hf** and BTZ in *Sa*ClpP are also shown. (d, e) Binding mode of the **43Hf** (d) and BTZ (e) interactions with critical residues of *Sa*ClpP. Residues that form hydrogen bonds with the ligand are shown as sticks and are labeled. (f) Comparison of the position of

His123 in tetradecameric wild-type *Sa*ClpP (PDB: 3V5E) [in pink], in heptameric *Sa*ClpP (PDB: 3ST9) [in light yellow], and in *Sa*ClpP with **43Hf** bound [in blue].

Like the β-lactone D3 and phenyl ester-containing compound ML90, which also covalently bound to the ClpP active site and resulted in retention of the tetradecameric assembly,[12,32,43] the boronate compounds did not lead to *Sa*ClpP disassembly. However, the insight into the mechanism of compounds triggering or disrupting the oligomerization remains to be elucidated. As previously proposed, the conserved active site histidine is critical in a hydrogen bonding network that is important for maintaining the oligomerization state, and alerting the orientation of its side chain causes deoligomerization.[44] In the boronate-bound *Sa*ClpP structures, the hydroxyl of boronic acid formed a hydrogen bond with the nitrogen atom of the His123 imidazole ring and kept this residue in place (Fig. 6f).

**Attenuation of *S. aureus* virulence by optimized compounds *in vitro* and *in vivo***

To identify a pharmacological candidate, we examined the activity of the optimized compounds in cell-based studies and cytotoxicity tests. To determine the inhibitory effects of boronate compounds on *S. aureus* growth, we measured the bacterial growth rate in the presence of different inhibitors. Compounds **43Hf** and **5Hf** demonstrated only minor inhibitory activity of bacterial growth of methicillin-resistant *S. aureus* (MRSA) ATCC33591 at concentrations up to 64 μM (Figs. 7a and S9). In cytotoxicity assays, **5Hf** showed moderate inhibition of HepG2

cells with a $GI_{50}$ value of 54.81 μM, but the other boronates displayed lower cytotoxicity toward HeLa and HepG2 cell lines (Table 1; Fig. S11).

Since ClpP controls the expression of bacterial Hla, which can cause cystitis, pyelonephritis, and sepsis[45], we treated MRSA with various concentrations of the boronate inhibitors and incubated the culture supernatants with erythrocytes to assess the level of secreted Hla. The boronate inhibitors themselves (other than MLN9708) showed no hemolytic activity even at 500 μM (Table 1). They all resulted in an obvious reduction in hemolysis caused by pretreated MRSA supernatant, with $IC_{50}$ values ranging from 1.4 to 23.5 μM (Fig. 7b; Table 1). **43Hf** was the best compound, approximately 30-fold more potent than BTZ. Western-blotting assays confirmed its downregulatory effect on the levels of Hla in the bacteria (Fig. S12). **43Hf** could almost eliminate Hla at 16 μM after the supernatant was concentrated 25-fold (Fig. 7c). To confirm the requirement of functional ClpP for **43Hf** inhibiting the Hla, we next investigated a ClpP-deletion (Δ*clpP*) strain and a complemented Δ*clpP*/pYJ335::*clpP* (Δ*clpP*$^+$) strain of *S. aureus* NCTC8325. We found that the hemolytic activity of the Δ*clpP* strain was greatly reduced compared with that of the wild-type (WT), and was not affected by the presence of **43Hf** (Fig. 7d). The WT and the complemented (Δ*clpP*$^+$) strains showed nearly identical hemolytic activity, and **43Hf** could suppress the production of Hla by these strains in a concentration-dependent manner (Fig. 7d). These results indicated that functional ClpP was a requirement for attenuation of *S. aureus* virulence by **43Hf**. Thus, we conclude that **43Hf** is a potent antivirulence candidate with a mild antibacterial effect

(minimum inhibitory concentration = 64–128 μg/mL) and low cytotoxicity.

To gain more detailed insight into the virulence inhibition activity of **43Hf**, we next determined the expression of several important virulence-related genes in *S. aureus* after **43Hf** treatment. According to quantitative polymerase chain reaction (qPCR) results (Fig. 7e), RNAIII effector, which controls a large number of virulence factors including Hla, was significantly repressed (>10-fold) by 16 μM **43Hf**. Expression of agrB, the agr quorum-sensing regulator, was reduced around 2-fold. Compound **43Hf** also demonstrated significant repression effects on expression of genes encoding toxins (hla, psm, lukS) and protease (aur).[45,46]

Cellular thermal shift assay (CETSA) was performed to confirm that **43Hf** engaged *Sa*ClpP in bacteria. CETSA monitors ligand-induced changes in thermal stability of a target protein to determine the binding affinity of the inhibitor for the target protein in whole cells.[47] Figure 7f showed that the *Sa*ClpP protein was unstable at 59 °C in MRSA treated with DMSO. The thermal stability of the endogenous *Sa*ClpP was enhanced by 100 μM **43Hf**; the protein remained stable even at 83 °C (Fig. 7f). These results provided direct evidence that **43Hf** is able to target *Sa*ClpP in bacteria.

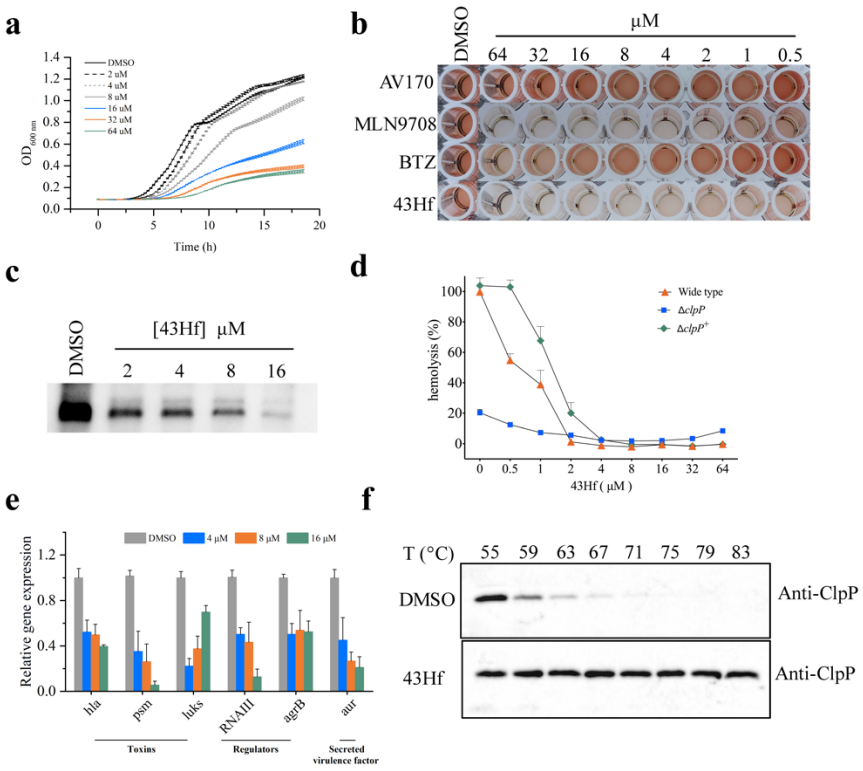


**Figure 7.** Compound **43Hf** affected the virulence of *S. aureus* virulence *in vitro*. (a) Growth curves of MRSA treated with various concentrations of **43Hf** in MHB medium. (b) The hemolytic activity of MRSA was reduced by **43Hf**. The images represent the released hemoglobin of in supernatant from mixtures of culture supernatant and sheep red blood cells after incubation for 1 h. (c) Western blot showing the production of Hla (25-fold concentrated) in **43Hf**-treated MRSA. (d) Comparison of the hemolytic activity of *S. aureus* WT, Δ*clpP* and complemented Δ*clpP*$^{+}$ treated with 43Hf at different concentrations. (e) Expressions level of the virulence genes (*hla*, *psm*, *luks*, *RNAIII*, *agrB* and *aur*) in MRSA in response to **43Hf** treatment. (f) CETSA of *Sa*ClpP in MRSA in the absence or presence of **43Hf**. The MRSA culture was incubated with 100 μM **43Hf** for 2 h before performing CETSA. The error bars of panels (a), (d) and (e) represent SD in three independent replicate

determinations.

*In vivo* efficacy of compound **43Hf** was evaluated using a murine skin abscess mice model generated by infection with MRSA ATCC33591. Different bacterial recovery levels from skin were observed between the control groups and the treated mice ($p=0.024$ for vehicle and 1.5 mg/kg **43Hf**, and $p=0.013$ for vehicle and 3 mg/kg **43Hf**) (Fig. 8a). The body weights of the mice were monitored daily, and **43Hf** caused no evident weight loss or other signs of adverse effects in the efficacy experiment (Fig. 8b). Serum biochemistry analyses were also performed to assess the potential toxicity. As shown in Figure S13, the kidney indicators creatinine (CREA), uric acid (UA) and blood urea nitrogen (BUN), and the heart indicator lactate dehydrogenase (LDH) maintained at normal levels. **43Hf** treatment increased the level of direct bilirubin (DBIL) and aspartate transaminase (AST) on day 4 but these returned to the normal level on day 14. All other hepatic indicators (albumin (ALB), total protein (TP), alkaline phosphatase (ALP) and alanine transaminase (ALT)) remained in the normal range. These findings demonstrated that **43Hf** may affect the hepatic function in the short term after administration, but without long-term impact.

Skin tissue and major organs (heart, liver, spleen, lung and kidney) were fixed in 4% paraformaldehyde, embedded, thin-sectioned and stained with hematoxylin and eosin (H&E). Pathological damages to skin tissue such as thickened dermis and inflammatory cell infiltration of the dermis was observed in the MRSA-infected group compared with the control (PBS treated groups) (Fig. 8c). Skin integrity

was preserved in mice treated with **43Hf** after the infection, and vancomycin (Van)-treated infected skin showed minimal inflammation (Fig. 8c). The MRSA infection caused severe alveolar destruction and interstitium thickening in the lung tissue of the vehicle group as *S. aureus* usually spread to the lung through the blood from skin,[48] while treatment with **43Hf** and Van obviously reduced the changes (Fig. S14). H&E stained sections of heart, liver, kidney and spleen revealed no histopathological changes (Fig. S14). All of these results demonstrated that **43Hf** was efficacious in attenuating the virulence of MRSA *in vivo*.

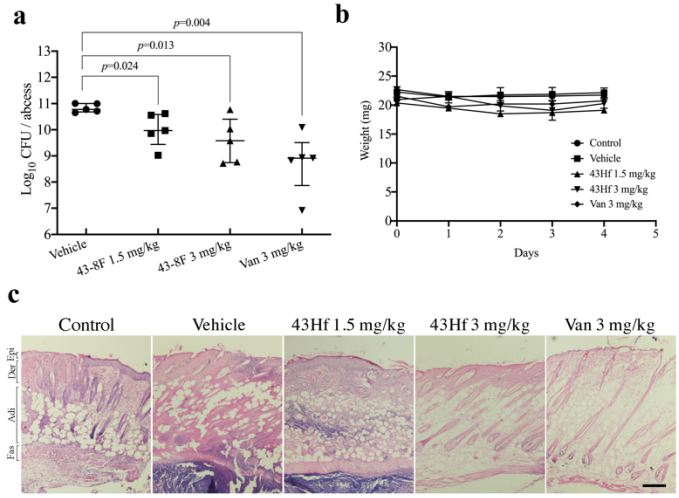


**Figure 8.** *In vivo* anti-virulence activity of compound **43Hf** in a mouse model of MRSA skin infection. (a) Bacterial counts in skin samples (n=5 mice/ group). The *p* value *vs* the vehicle group determined with *t*-test. (b) Animal body weight change. Data are represented as the mean ± SD (n=5 mice/ group). (c) H&E stained of infected skin on day 4 after the first administration of treatment were analyzed by microscopy. Scale bar 200 μm.

## Discussion and Conclusions

The traditional small-molecule drug discovery process is still costly and time-consuming, involving iterative rounds of molecular design, chemical synthesis, biological assay, and data analysis. The relatively large consumption of chemical materials, hazardous workup, low signal-to-noise outputs, and cumbersome equipment required for recent techniques make new drug development increasingly difficult. In this study, we describe a low-cost and simple combinatorial approach that consolidated computational ranking, multistep miniaturized synthesis in microplates, and cascaded bioactivity testing for rapid exploration of preliminary SARs of inhibitor compounds of *Sa*ClpP. The coupled miniaturized synthesis (<0.1 mg of reactants for each reaction) enabled parallel synthesis of large collections of compounds with minimal consumption. The cascaded *Sa*ClpP inhibition assay directly screened out active compounds from the crude products without time-intensive and laborious reaction purification.

Nevertheless, we cannot avoid false negative hits in this integration platform of synthesis and testing because the reaction yield depends on the starting materials and intermediates to some extent. Importantly, our combinatorial and focused compound library exploration and enzymatic screening identified five compounds suitable for scaled-up synthesis. Eventually, from these five active *Sa*ClpP inhibitors, compound **43Hf** was proved to be a promising submicromolar inhibitor of *Sa*ClpP that is capable of targeting endogenous ClpP in bacterial cells. Several specific ClpP inhibitors have been developed to decrease the virulence of bacteria and be used in combination

with existing antibiotics. β-Lactones (D3 and U1)[11,49] and a phenyl esters (AV170)[12] can covalently bind to the active-site serine, but the low stability of the electrophilic motif (cyclic ester and phenol ester, respectively) impeded their further application. Moreover, a noncovalent oxazole inhibitor (AV145)[13] was reported to bind to the handle region of ClpP, but it was not efficient in inhibition of intracellular Hla. A β-sultam (RSK07)[32] could convert the active site serine of ClpP into a dehydroalanine, however, the reaction proceeded rapidly in other proteins, such as β-lactamases, and might lead to indiscriminate protein modification and toxicity. The first covalent inhibitor of *Ec*ClpP, Z-LY-CMK,[18] showed low activity with an $IC_{50}$ value of 14.4 μM. Subsequently, an α-amino diphenyl phosphonates (DDP85)[19] was developed with a submicromolar $IC_{50}$ against *Ec*ClpP, but could it only show reduction of growth of WT *E. coli* under nitric oxide stress at up to 100 μM. The boronate warhead of **43Hf** was considered to be an appropriate covalent binder, based on the success of analogues binding to *Mt*ClpP[14,15] and *h*ClpP.[16] The reversible covalent binding mode of **43Hf** has advantages over the irreversible inhibitors, such as enabling optimization of the inhibitor residence time. Benefiting from the high antivirulence efficacy *in vitro* and *in vivo,* **43Hf** is considered a good option for further investigation.

In sight of the binding mode of **43Hf** with *Sa*ClpP (Fig. 6), the boronate underwent nucleophilic attacked by the active-site residue Ser98 to form an anionic tetrahedral structure. The crystal structure indicated that boronate compounds with aromatic methyl moieties at positions I and II, which fit between strands β3 and β9 of *Sa*ClpP, displayed stronger inhibitory activity. The boronate compound showed reversible

covalent binding with the ClpP active site and did not lead to disassembly of the *Sa*ClpP tetradecamer. The mechanism of ClpP inhibition by β-sultams was reported to be disruption of the oligomer, but they mainly employed the way of inducing dehydroalanine (Dla) formation of the active site Ser98[32]. The covalent inhibitors β-lactones D3 and phenyl esters ML90 also retained the tetradecameric structure of ClpP and the binding mode was investigated by molecular docking and CID-MS.[12,32,43,50] In this study, the crystal structure of the *Sa*ClpP–**43Hf** complex shows directly that a hydrogen bond formed between a hydroxyl group of boronic acid and the nitrogen atom of the imidazole ring of His123 might explain retention of the tetradecameric structure of ClpP because of the critical role of this histidine in the deoligomerization process.[44]

In conclusion, this work has validated the effectiveness of an integrated strategy for hit optimization. Integration of in silico position scanning, multistep miniaturized synthesis and cascaded bioassays in microplates allowed us to rapidly explore SAR and obtain several potent *Sa*ClpP inhibitors. Compound **43Hf** is promising for further investigation and even pharmaceutical development because of its capability of binding intracellular ClpP, and attenuation of MRSA virulence *in vitro* and *in vivo*. For side effects of compound **43Hf**, the hypodermic injection of compound **43Hf** could affect the hepatic indicators in the short term, but return to normal after drug withdrawal. No histopathological damage of the major organs was observed in pharmacodynamic experiments. The boronate-bound *Sa*ClpP crystal structure explained the noncanonical ClpP inhibition mechanism, in which the

covalent binding of boron with serine stabilized the tetradecameric assembly of *Sa*ClpP. Finally, the new insights gained in this study provide a rational design direction for developing covalently-binding inhibitors of ClpP. As the boronate inhibitors showed poor selectivity of 20S proteasome and the homologous *h*ClpP and *Pa*ClpP1, future studies could consider modification of inhibitors to target the allosteric site of ClpP in order to improve species and target selectivity.

## Experimental Section

**General Methods.** All common chemicals and solvents were purchased from bidepharm (China) and were used without further purification. Analytical thin layer chromatography (TLC) was silica gel 60 F254 precoated plates (0.25 mm, Qingdao Haiyang Ltd., China) and components were visualized by ultraviolet light (254 nm). Silicycle silico gel 300-400 (particle size 40-63 μm) mesh was used for all flash column chromatography experiments. All NMR spectrum were recorded on a Bruker Avance (Varian Unity Inova) 400 MHz spectrometer in DMSO-$d_6$ with TMS as internal standard. $^{1}$H NMR and $^{13}$C NMR were analyzed by MestReNova Software. Mass spectrometric data were obtained on a Waters Acquity UPLC H-Class / SQD2 system and the ESI detector produced positive ion (+) as well as negative ion (-) spectra. Waters e2695 HPLC system was used to analyze the final compounds with DAD at 270 nm (Column: Venusil XBP C18 reversed-column (4.6 mm × 250 mm, 5 μm); mobile phase A: water + 0.1 % formic acid; mobile phase B: ACN + 0.1 % formic acid; flow rate: 1 mL/min; gradient: 30% B at 0 min, 30 %B at 5 min, 90% B

at 20 min, 90 % B at 30 min). All final compounds submitted to the biology assays were determined to be ≥95% purity using the area normalization method. The Mueller-Hinton broth (MHB), cation-adjusted MHB (CAMHB) and tryptone soy broth (TSB) were purchased from BD Difco. Fluorescent substrates Ac-WLA-AMC and Abz-T-V-A-W-pNA were synthesized by GL Biochem Shanghai Ltd. (China). MRSA ATCC 33591was obtained from American type culture collection. Sheep erythrocytes were used for hemolysis assay. The rabbit polyclonal anti-ClpP antibody was generated by Sangon Biotech (China) using purified ClpP.

**Implementation of multi-step miniaturized synthesis.** All reactions were carried out in 96-well microtiter plates at 100 μL scale. All the substrates were dissolved in dry DMSO to give an appropriate concentration. The reactants were added to the well with a certain amount of equivalence followed by the appropriate reaction solvent and the final concentration of reactants (1 eq.) were 100 mM. After dispensing the reaction plates were sealed and allowed to shake at RT overnight. The reaction mixtures were extracted with DCM and transferred in Eppendorf tubes. The DCM extracts were dried by nitrogen and re-dissolved in solvent to give a product mixture solution of Σ[Pn] = 100 mM for next-step reaction or inhibition testing.

**General procedure A for the synthesis of intermediates 3a~3e.** To a solution of corresponding aromatic carboxylic acid (2,5-dichlorobenzoic acid, 2-(4-isobutylphenyl) propanoic acid, 4-methoxy-2-methylbenzoic acid, 4-methoxybenzoic acid) (1 eq.) in DCM, triethylamine (1.4 eq.) and 2-(7 -azabenzotriazol-1-yl)-*N*, *N*, *N*', *N*'-tetramethyluronium hexafluorophosphate (HATU)

(1.3 eq.) were added. The reaction mixture was stirred at RT for 10 min, then corresponding α-amino acid methyl esters (methyl *L*-tryptophanate, methyl *L*-tyrosinate, methyl *L*-phenylalaninate) (1.1 eq.) was added into the reaction mixture. The resulting mixture was stirred at RT for 8~10 h. After the reaction was complete, the mixture was washed with brine for 3 times and evaporated under vacuum to remove solvent to give crude products **3a**~**3e**, which was used directly in the next step.

**General procedure B for the synthesis of intermediates 4a~4e.** To a solution of corresponding intermediates (**3a**~**3e**) (1 eq.) in THF/MeOH/$H_2O$ (1:1:1), LiOH (2.5 eq.) was added. The resulting mixture was stirred at 0 °C for 4~8 h. Then the mixture was buffered to pH 1~2 with 37 % hydrochloric acid and extracted with DCM for 7~8 times. The combined organic layer was dried with anhydrous sodium sulfate and was evaporated under vacuum to remove solvent to give crude products **4a**~**4e**, which was used directly in the next step.

**General procedure C for the synthesis of intermediates 6a~6e.** To a solution of corresponding intermediates (**4a**~**4e**) (1 eq.) in DCM, triethylamine (1.4 eq.) and 2-(7-azabenzotriazol-1-yl)-*N*,*N*,*N*',*N*'-tetramethyluronium hexafluorophosphate (HATU) (1.3 eq.) were added. The reaction mixture was stirred at RT for 10 min, then (*R*)-3-methyl-1-((3a*S*,4*S*,6*S*,7a*R*)-3a,5,5-trimethylhexahydro-4,6-methanobenzo[*d*][1,3,2]dioxaborol-2-yl)butan-1-amine (1.1 eq.) was added into the reaction mixture. The resulting mixture was stirred at RT for 8~10 h. After the reaction was finished, the mixture was washed with brine for 3

times and evaporated under vacuum to remove solvent to give crude products **6a**~**6e**, which was used directly in the next step.

**General procedure D for the synthesis of compounds 5Bf, 5Hf, 11Qf, 24Qf and 43Hf.** To a solution of corresponding intermediates (**6a**~**6e**) (1 eq.) in EA/MeOH (10:1), 10 M aqueous HCl and *iso*-butylboronic acid (5 eq.) was added. The resulting mixture was stirred at RT for 12 h. After the reaction was finished, the organic layer was separated and the aqueous layer was extracted with EA for three times, the combined organic layer was dried with anhydrous sodium sulfate and evaporated under vacuum to remove solvent to give crude product, which was purified through silica gel column to afford compounds **5Bf, 5Hf, 11Qf, 24Qf and 43Hf**.

**((1*R*)-1-((2*S*)-3-(4-hydroxyphenyl)-2-(2-(4-isobutylphenyl)propanamido)propa namido)-3- methylbutyl)boronic acid (5Bf).** Stepwise following general procedure *A*, *B*, *C* and *D*, beginning with starting materials 2-(4-isobutylphenyl)propanoic acid and methyl *L*-tyrosinate to afford compound **5Bf** as a white solid (total yield of four steps: 17.7%). $^{1}$H NMR (400 MHz, DMSO-$d_6$) δ 9.10 (m, 1H), 8.57 (m, 1H), 8.11 (m, 1H), 7.11 (m, 1H), 7.01 (m, 4H), 6.80 (m, 1H), 6.62 (d, $J$ = 7.6 Hz, 1H), 6.50 (m, 1H), 4.40 (m, 1H), 3.57 (mz, 1H), 2.88 (m, 1H), 2.69 (m, 2H), 2.38 (m, 2H), 1.79 (m, 1H), 1.51 (m, 1H), 1.25 (m, 5H), 0.84 (m, 12H). $^{13}$C NMR (100 MHz, DMSO-$d_6$) δ 173.81, 156.36, 139.54, 139.41, 130.71, 130.60, 130.56, 129.11 (2C), 127.53, 127.49, 127.40, 115.29 (2C), 44.76, 30.07, 30.05, 25.57, 25.49, 23.54, 22.90, 22.69 (2C), 22.66 (2C), 19.17, 18.40. LC/MS: calculated for $C_{27}H_{39}BN_2O_5$ [M]: 482.2952, found $[M\text{-}OH^-]^+$: 465.43. HPLC: $t_R$=12.129 min (98.96%).

**((1*R*)-1-((2*S*)-3-(1*H*-indol-3-yl)-2-(2-(4-isobutylphenyl)propanamido)propanamido)-3-methylbutyl)boronic acid (5Hf).** Stepwise following general procedure *A*, *B*, *C* and *D*, beginning with starting materials 2-(4-isobutylphenyl)propanoic acid and methyl *L*-tryptophanate to afford compound **5Hf** as a pale yellow solid (total yield of four steps: 19.0%). $^{1}$H NMR (400 MHz, DMSO-$d_6$) δ 10.75 (m, 1H), 8.57 (m, 1H), 8.16 (m, 1H), 7.50 (m, 1H), 7.29 (m, 1H), 7.01 (m, 7H), 4.55 (m, 1H), 3.60 (m, 1H), 3.05 (m, 2H), 2.64 (m, 1H), 2.34 (m, 2H), 1.76 (m, 1H), 1.54 (m, 1H), 1.29 (m, 5H), 0.82 (m, 12H). $^{13}$C NMR (100 MHz, DMSO-$d_6$) δ 173.99, 145.21, 139.53, 136.51, 129.12 (2C), 127.78, 127.47, 127.44, 127.35, 121.82, 121.24, 118.82, 118.74, 111.72, 104.66, 44.77, 30.04, 25.66, 25.63, 25.57, 23.53, 23.08, 22.69 (2C), 22.64 (2C), 19.07, 11.10. LC/MS: calculated for $C_{29}H_{40}BN_3O_4$ [M]: 505.3112, found $[M\text{-}OH^-]^+$: 488.20. HPLC: $t_R$=16.318 min (96.76%).

**((R)-1-((S)-2-(4-methoxy-2-methylbenzamido)-3-phenylpropanamido)-3-methylbutyl) boronic acid (11Qf).** Stepwise following general procedure *A*, *B*, *C* and *D*, beginning with starting materials 4-methoxy-2-methylbenzoic acid and methyl *L*-phenylalaninate to afford compound **11Qf** as a white solid (total yield of four steps: 15.1%). $^{1}$H NMR (400 MHz, DMSO-$d_6$) δ 8.76 (m, 1H), 8.32 (m, 1H), 7.28 (m, 6H), 6.70 (m, 2H), 4.72 (m, 1H), 3.71 (m,3H), 3.12 (m, 1H), 2.92 (m, 1H), 2.69 (m, 1H), 2.13 (m, 3H), 1.61 (m, 1H), 1.35 (m, 1H), 1.26 (m, 1H), 0.86 (m, 6H). $^{13}$C NMR (100 MHz, DMSO-$d_6$) δ 174.31, 169.07, 160.42, 138.57, 137.98, 129.75 (2C), 129.40, 128.95, 128.51 (2C), 126.83, 116.26, 110.79, 55.56, 52.35, 37.53, 25.58, 23.58, 23.13,

23.08 (2C), 20.16. LC/MS: calculated for $C_{23}H_{31}BN_2O_5$ [M]: 426.2326, found $[M\text{-}OH^-]^+$: 409.30. HPLC: $t_R$=11.955 min (97.19%).

**((*R*)-1-((*S*)-2-(4-methoxybenzamido)-3-phenylpropanamido)-3-methylbutyl) boronic acid (24Qf).** Stepwise following general procedure *A*, *B*, *C* and *D*, beginning with starting materials 4-methoxybenzoic acid and methyl *L*-phenylalaninate to afford compound **24Qf** as a white solid (total yield of four steps: 15.8%). $^1$H NMR (400 MHz, DMSO-$d_6$) δ 8.78 (m, 1H), 8.48 (m, 1H), 7.70 (m, 2H), 7.26 (m, 5H), 6.94 (m, 2H), 4.70 (m, 1H), 3.77 (m, 3H), 3.05 (m, 2H), 2.62 (m, 1H), 1.57 (m, 1H), 1.28 (m, 2H), 0.84 (m, 6H). $^{13}$C NMR (100 MHz, DMSO-$d_6$) δ 174.32, 166.23, 162.15, 138.15, 129.79, 129.71 (2C), 129.66, 128.51 (2C), 126.77, 126.49, 113.79 (2C), 55.78, 52.73, 37.47, 25.54, 23.50, 23.47, 23.14, 22.64. LC/MS: calculated for $C_{22}H_{29}BN_2O_5$ [M]: 412.2170, found $[M\text{-}OH^-]^+$: 396.32. HPLC: $t_R$=11.485 min (98.84%).

**((*R*)-1-((*S*)-2-(2,5-dichlorobenzamido)-3-(1*H*-indol-3-yl)propanamido)-3-methylbutyl) boronic acid (43Hf).** Stepwise following general procedure *A*, *B*, *C* and *D*, beginning with starting materials 2,5-dichlorobenzoic acid and methyl *L*-tryptophanate to afford compound **43Hf** as a pale yellow solid (total yield of four steps: 23.1%). $^1$H NMR (400 MHz, DMSO-*d6*) δ 10.85 (d, J = 1.6 Hz, 1H), 8.80 (d, J = 8.4 Hz, 1H), 8.71 (m, 1H), 7.60 (m, 1H), 7.45 (m, 2H), 7.32 (m, 1H), 7.19 (m, 2H), 7.06 (m, 1H), 6.96 (m, 1H), 4.78 (m, 1H), 3.26 (m, 1H), 3.11 (m, 1H), 2.73 (m, 1H), 1.65 (m, 1H), 1.44 (m, 1H), 1.29 (m, 1H), 0.85 (m, 6H). $^{13}$C NMR (100 MHz, DMSO-*d6*) δ 173.99, 165.29, 138.00, 136.54, 131.83, 131.76, 131.08, 129.45, 129.03, 127.76, 124.43, 121.35, 118.88, 118.75, 111.73, 109.80, 52.08, 49.08, 27.73, 25.65,

23.57, 23.17, 22.64. LC/MS: calculated for $C_{23}H_{26}BCl_2N_3O_4$ [M]: 489.1393, found $[M\text{-}OH^-]^+$: 472.15. HPLC: $t_R$=11.515 min (99.55%).

**Molecular docking.** The combinatorial virtual library was constructed by the amino condensation reaction in Discovery Studio software. The extended form of *Sa*ClpP structure (PDB: 3V5E) were used for docking. The compounds in the library and the protein were subjected to a standard prepared workflow in Schrödinger suite. All compounds were docked into the catalytic site using the Gilde XP docking procedure and the GlideGscore were utilized to rank the compounds versus the hit MLN2238.

**Protein expression and purification.** Full length *S. aureus* ClpP, *P. aeruginosa* ClpP1, *S. aureus* ClpX and human ClpP (57-277) with N-terminal His6-sumo-tag was cloned in pRSF Duet1 and expressed and purified as described with slight modifications.[12,39] The pRSF Duet1 plasmid containing *Sa*ClpP, *h*ClpP, *Pa*ClpP1 or *Sa*ClpX was transformed into the *E. coli* host strain BL2 (DE3) (Invitrogen). The bacterial culture was grown in LB in the presence of 50 μg/mL kanamycin at 37 °C. After an $OD_{600}$ (ZhiChu Instrument Ltd., China) of approximate 0.8 was achieved, the culture was cooled to 16 °C and then induced with 0.1 mM isopropyl β-D-1-thiogalactopyranoside (IPTG) for 16 h. Following induction, the bacteria were collected and resuspended in lysis buffer consisting of 25 mM Tris-HCl pH 8.0, 150 mM NaCl. After lysed by sonication, the lysate was centrifuged at 15,000 rpm for 45 min and then the supernatant was loaded onto a Ni-NTA column (Qiagen) pre-equilibrated with a binding buffer (25 mM Tris-HCl pH 8.0 and 150 mM NaCl).

The column was washed with the binding buffer supplemented with 20 mM imidazole for 10 column volumes, and the protein on the Ni-NTA resin was eluted with the binding buffer supplemented with 300 mM imidazole. The tag was removed by Ulp1 and the purified untagged *h*ClpP, *Pa*ClpP1 and *Sa*ClpX were further concentrated using a Centricon filter (10kDa cutoff, Millipore) and stored at -80 °C, respectively. The *Sa*ClpP samples were subjected to anion exchange (MonoQ, GE Healthcare) and size exclusion chromatography using (Superdex 200, GE Healthcare). Fractions containing *Sa*ClpP were pooled and concentrated to a concentration of approximately 10 mg/mL using a Centricon filter and stored at -80 °C.

The AlgW was amplified from the P. aeruginosa genomic DNA by PCR using gene-specific primers and inserted into plasmid pET22b-His6 by ClonExpress II One Step Cloning Kit (Vazyme). The pET22b-AlgW-His6 was transformed into E. coli BL21 (DE3). The bacterial were grown in LB medium in the presence of 100 μg/mL ampicillin at 37 °C, and protein expression was induced with 0.1 mM IPTG under 16 °C for 15 h until the $OD_{600}$ reached about 0.8-1. Bacteria were collected and resuspended in lysis buffer consisting of 25 mM Tris–HCl pH 7.5, 150 mM NaCl, 5% glycerol. After lysed by sonication, the supernatant was obtained by centrifugation at 15,000 rpm for 30 min and then co-incubated with 4 mL Ni–NTA affinity resin (Qiagen) for 1 h. The mixture was washed with lysis buffer supplemented with 25 mM imidazole and the target proteins were eluted with lysis buffer containing 300 mM imidazole. The protein was further purified with size-exclusion chromatography Superdex-200 column with a solution of 25 mM Tris-HCl pH 7.5, 150 mM NaCl.

Peak fractions were pooled and concentrated to a concentration of approximately 10 mg/mL using a Centricon filter and ultimately stored at -80 °C.

**Library screening.** 1 μM *Sa*ClpP was dissolved in the assay buffer and incubated with each compound (final concentration of 10 μM) or DMSO in a black flat bottom 96-well plates (corning) at 37 °C for 10 min. The fluorogenic substrate N-succinyl-Leu-Tyr-amido-4-methylcoumarin (Suc-LY-AMC) was then added to each well (final concentration of 200 μM). After 1 h incubation, fluorescence was measured at 380/440 nm in the Cytation imaging reader (Biotek). 2632 compounds were screened and the inhibition ratio was calculated based on the method that fluorescence was normalized to the DMSO control (100% activity). Experiments were performed once with triplicate wells.

**Enzymatic assays.** For ClpP peptidase inhibition assay, the buffer solution for *Sa*ClpP consisted of 100 mM Hepes, pH 7.0, 100 mM NaCl, for *h*ClpP consisted of 25mM Tris-HCl, pH 8.0, 100 mM KCl, and for *Pa*ClpP1 consisted of 25mM Tris-Cl, pH 7.5, 150 mM NaCl. The dose response analysis was carried out using a two-fold dilution series over 8 steps starting at 100 μM (*Sa*ClpP and *h*ClpP) or 50 μM (*Pa*ClpP1). 1 μL inhibitor (stock in DMSO) or 1 μL DMSO for the control group was added in a black flat bottom 96-well plat and mixed with 98 μL enzyme solution (final ClpP monomer concentration of *Sa*ClpP: 1 μM, *h*ClpP: 3.5 μM, *Pa*ClpP1: 0.5 μM). The mixture was incubated at RT for 10 min and the reaction was initiated by addition of 1 μL substrate (*Sa*ClpP: 200 μM Suc-LY-AMC, *h*ClpP: 100 μM Ac-WLA-AMC, *Pa*ClpP1: 50 μM Suc-LY-AMC). Fluorescence was recorded at 380/440 nm for 1 h at

37 °C and the slope of the curves was determined in the software of GraphPad Prism 8. The DMSO control samples were normalized to 100% activity and the $IC_{50}$ was calculated from the nonlinear regression curve fit using GraphPad Prism 8. For the substrate competition assay of *Sa*ClpP, the final concentration of substrate up to 1 mM was added. For the time-course inhibition assay of *Sa*ClpP, the inhibitors were pre-mixed with 200 μM substrate Suc-LY-AMC, and the reaction was started by adding 1 μM *Sa*ClpP protein. The $K_i$ and $k_{inact}$ were calculated through a least squares fit by XLFit software. Experiments were performed thrice with triplicate wells in each experiment.

For the protease activity assay, the buffer solution consisted of 25 mM Hepes, pH 7.5, 20 mM $MgCl_2$, 30 mM KCl, 0.03% Tween 20, 10% glycerol, 2 mM DTT. Each ClpXP reaction contained 3.6 μM *Sa*ClpP, 3 μM *Sa*ClpX and an ATP-regenerating system (4 mM ATP, 20 U/mL creatine kinase and 16 mM creatine phosphate). 0.048 mg/mL FITC-casein was then added to each well and the fluorescence was measured at 494/521 nm for 50 min. The slope of fluorescence (300- 1200 s) were used for the calculation of inhibition ratio and the DMSO control was normalized to 100 % activity. Experiments were performed thrice with triplicate wells in each experiment.

The 20S proteasome inhibition assay was performed by Medicilon Corporation (China). Compounds MLN9708, **5Bf**, **24Qf and 43Hf** were tested in three-fold dilution series over 10 steps starting at 1 μM. The 20S proteasome enzyme (2 nM) was treated with the inhibitors in reaction buffer (25 mM Hepes, pH 7.5, 5 mM EDTA, 0.5% NP-40, 0.02% SDS), then the substrate Suc-LLVY-AMC (final

concentration of 10 μM) was added into the mixture and co-incubated at RT for 1 h. Fluorescence was measured at 360/460 nm and the percentage enzyme activity was calculated based on the fluorescence comparing to the DMSO control (100% activity). The $IC_{50}$ was determined from the nonlinear regression curve fit using GraphPad Prism 8. Experiments were performed thrice with triplicate wells in each experiment.

The inhibition of AlgW activity was determined using the quenched fluorescent substrate Abz-T-V-A-W-pNA. The enzyme was diluted with assay buffer (25 mM Tris, pH 7.5, 150 mM NaCl) and treated with SVRDELRWVF peptide for 30 min at 37 °C. 100 μM inhibitors were incubated in the solution containing 200 nM AlgW and 10 mM SVRDELRWVF at RT for 10 min. The reaction was initiated by adding 100 μM Abz-T-V-A-W-pNA and fluorescence was measured at 310/420 nm at 1 min intervals for 1 h. The slope of the curves was determined in the software of GraphPad Prism 8 and the inhibition ratio was normalized to DMSO control (100% activity). Experiments were performed once with triplicate wells.

The FXa inhibition assay was performed by Medicilon Corporation (China). 100 μM inhibitors were incubated with FXa (Abcam, final concentration of 30 nM) in assay buffer (50 mM Tris-HCl, pH 8.4) at RT for 10 min. Following that, the chromogenic substrate Pefachrome Fxa was added into the mixture and co-incubated at RT for 20 min. The absorbance at 405 nm was measured and the percentage enzyme activity was normalized to the DMSO control (100% activity). Experiments were performed once with triplicate wells.

**Thermal shift assay.** The DSC measurement were carried out on a Microcal VP-Capillary DSC (Malvern). 0.5 mg/mL (25 μM) *Sa*ClpP was incubated with 100 μM inhibitors or two-fold dilution series of inhibitors at RT in a total volume of 400 μL assay buffer. Scans were performed at 1 °C/min in the 30-90 °C temperature range. A buffer-buffer scan, under the same conditions, was subtracted from the corresponding buffer-sample endotherm scan and the baseline was draw for each scan. $T_m$ values were corresponding to the maximum of each thermogram peak. Experiments were performed once with single well.

The DSF assay was conducted as previously described.[51] In short, *Sa*ClpP was dissolved in the assay buffer (100 mM Hepes, pH 7.0, 100 mM NaCl, final concentration of 2 μM) and incubated with 50 μM inhibitors (or two-fold dilution series of **43Hf**) or DMSO as a control for 30 min. 25 μL 10 × SYPRO orange (Thermo) was mixed with protein solution and added to the white PCR 8 strip tubes. The assay was performed using the CFX96 Real-time System (BioRad) while heating from 25 °C to 99 °C in 0.5 °C steps. The data were processed with CFX Manager software and GraphPad Prism 8. Experiments were performed thrice with duplicate wells in each experiment.

**Isothermal titration calorimetry.** The ITC experiments were performed on a MicroCal iTC200 system (GE Healthcare) and with constant stirring at 500 rpm. The experiment was started after equilibration for 150 s with a first injection of 1 μL which was discarded during the analysis. A typical experiment consisted of 19 subsequent injections with a 2 μL injection volume into a cell filled with 200 μL

sample. Each injection was made over a period of 5 s with a 2-3 min interval between subsequent injections. Power was recorded at 'high' gain setting, with a reference power of 7 μcal/s and a 5-s filter period. Data analysis including baseline correction and evaluation was carried out with OriginPro 8.5 ITC.

**Hemolysis assay.** MRSA ATCC 33591, *S. aureus* Newman strains (NCTC8325 (WT), Δ*clpP*,[39] Δ*clpP*/pYJ335::*clpP* (Δ*clpP*$^{+}$)[39] were cultured in MHB medium overnight, and then diluted into an $OD_{600}$ of 0.05. When shaken to an $OD_{600}$ of approximate 0.6 at 37 °C, the suspension was mixed with serial dilution inhibitors or DMSO as a control and the resultant bacterial continued growing for 8 h. The culture was harvested and supernatant was transferred to a tube, following that, the supernatant was mixed with 5 % sheep erythrocytes (10 mM Tris, pH 7.4, 0.9% NaCl) at 1:1 ration. The samples were then centrifuged at 1,500 rpm for 15 min. The released hemoglobin in the supernatant were transferred to the 96-well plates for imaging and the absorbance was measured at 545 nm. For determination of hemolytic activity of inhibitors, serial diluted inhibitors were directly mixed with 2% sheep erythrocytes, with the buffer solution as the negative control and with Milli-Q water as the positive control. The $EC_{50}$ values were determined by fitting to nonlinear regression analysis using GraphPad Prism 8. Experiments were performed thrice with triplicate tubes in each experiment.

**Reversibility assay.** 1 μM ClpP (100 mM Hepes, pH 7.0, 100 mM NaCl) were incubated with 20-fold molar excess of inhibitor or DMSO for 1 h at RT. The reaction was then transferred to dialysis cassettes (1 mL, 10 kDa MWCO) and dialyzed against

2 L buffer at 4 °C. Buffer was removed after first 6 h dialysis, and following that, buffer was removed after every 24 h until the end of experiment. 50 μL aliquots were removed for *Sa*ClpP peptidase activity assay as described above. Experiments were performed thrice with single sample in each experiment.

**Analytical gel filtration.** 25 μM ClpP was incubated with 125 μM inhibitors or DMSO as a control in a total volume of 200 μL buffer (100 mM Hepes, pH 7.0, 100 mM NaCl) for 1 h at RT. After centrifugation at 15,000 rpm for 10 min at 4 °C, the supernatant was subjected to a calibrated Superdex 20 Increased 10/300 GL column (GE Healthcare) connected to an Akta purifier 10 system (GE Healthcare). The column was flushed with 50 mL buffer (20 mM Hepes, pH 7.0, 100 mM NaCl) and the UV absorption was recorded at 280 nm which was normalized to the highest signal. Protein masses and oligomerization state were determined from the retention times according to the column manufacturer's manual and comparison of the elution volumes to ClpP treated with AV170.

**Native-PAGE assay.** The native-PAGE assay was performed using 10% acrylaminde gel. The 5 × native loading buffer was added to each sample and 10 μL aliquots were loaded on the gel. Electrophoresis was performed at 4 °C for 8 h with 1 h pre-cold. The high MW non-denaturing protein Marker (Coolaber, China) was used as a standard protein marker.

**Crystallization and structure determination. 43Hf** or BTZ-bound *Sa*ClpP complex crystals were carried out by the hanging drop vapor-diffusion method at 16 °C and mixing 1 μL protein with 1 μL well solution. 10 mg/mL *Sa*ClpP was

incubated with 4-fold molecular excess of **43Hf** or BTZ (2 mM) for 1 h at 16 °C. This solution was submitted to a high-throughput crystallization screening using commercially available 96-well kits: Wizard 1&2 and 3&4 (Rigaku), Crystal Screen (Hampton Research) and Index HT (Hampton Research). Well-diffracting crystals appeared after several days, drops contained equal volumes of protein solution and reservoir solution (0.1 M Sodium chloride, 0.1M HEPES pH 7.5 and 1.6 M Ammonium sulfate). Crystals were soaked for about 30 s in mother liquor adding 10 % glycerol and were stored in liquid nitrogen. The X-ray data were collected with a CCD camera on BL-18U station of the SSRF, Shanghai, China. Diffraction images were indexed and diffraction spots were integrated and scaled using the HKL2000 software package.[40] Structures were solved by molecular replacement with the program suite PHENIX.[52] Subsequent cycles of manual model rebuilding with COOT[53] and refinement with PHENIX improved the qualities of structural models before being deposited to the Protein Data Bank.

**Antibacterial test.** The antibacterial activity of compounds was determined by incubating MRSA at an inoculum of approximately $5\times10^5$ CFU/mL in 100 μL MHB liquid medium in 96-well plates. The cultures mixed with compounds at gradient concentrations were compared to cultures mixed with DMSO (negative controls). The bacterial growth curve was determined by measuring the optical density at 600 nm for 18 h. Experiments were performed thrice with triplicate wells in each experiment.

The minimal inhibitory concentration (MIC) of **43Hf** was determined in triplicate with the broth microdilution method according to the Clinical and

Laboratory Standards Institute (CLSI) guidelines. The MRSA was cultured in CAMHB and **43Hf** was diluted to different concentrations ranging from 0.5 to 256 μg/mL in 96-well plates to a volume of 90 μL. Bacteria were cultured overnight and diluted with CAMHB to $5 \times 10^6$ CFU/mL. 10 μL suspension culture was added to each well for the final inoculum of $5 \times 10^5$ CFU/mL. The MIC value was determined as the lowest concentration completely inhibiting visible growth of the bacteria after 18 h incubation at 37 °C. Experiments were performed thrice with triplicate wells in each experiment.

**Quantitative polymerase chain reaction (qPCR).** The total RNA of the MRSA was prepared thorugh liquid nitrogen freezing and thawing using $2 \times 10^8$ CFU bacteria, then purified using the TRIzol reagent (Thermo) according to the manufacturer's instructions. The RNA yield was assessed with a NanoDrop spectrophotometer (Thermo) and the quality of total RNA were confirmed by agarose electrophoresis. 1 μg of total RNA was converted to cDNA with a PrimeScript RT reagent Kit (Takara). The resulting cDNA was subjected to real-time PCR using TB Green Premix Ex Taq II (Takara) and the CFX96 Real-time System (BioRad). We analyzed selected genes using primers in Table S4. The relative quantification of the investigated genes was determined by the ratio of expression related to the endogenous control gyrase (gyrB). Experiments were performed thrice with triplicate wells in each experiment.

**Western blot.** All cultures treated with different inhibitors were diluted with PBS to the inoculum of $9.3 \times 10^7$ CFU/mL and 20 μL supernatant was added to each well

to compare the production of α-hemolysin in the supernatant. For the 25-fold concentrated samples, the culture supernatant was concentrated with 10 kDa concentrator (Millipore) and washed with PBS. Total protein concentration was around 0.9 mg/mL and 5 μL was added to the well. The western blotting experiment was performed following SDS-PAGE gel electrophoresis. The protein bands were transferred to a PVDF membrane and α-hemolysin was detected with polyclonal anti-staphylococcal α-Toxin antibody (Sigma-Aldrich) and AffiniPure goat HRP-conjugated anti-rabbit IgG (1:10,000) (ZenBio). The enhanced chemiluminescence (ECL) solution (Millipore) was used to autoradiography and the images were collected with ChemiScope 6100 Touch (Clinx, China).

**Cytotoxicity study.** Potential toxicity of the compounds in HeLa and HepG2 cells was evaluated by MTT assay according to the manufacture's guidelines. Briefly, $3 \times 10^3$ cells of HeLa and $4 \times 10^3$ cells of HepG2 in 100 μL DMEM medium were seed to each of the 96-well plates. After 24 h culturing, 100 μL DMEM medium with test compounds were transferred into the appropriate wells and further co-incubated for 24 h. Absorbance was read with a Microplate Reader (Thermo) at 570 nm with DMSO wells as the positive control. The average 50% growth inhibition concentration ($GI_{50}$) was determined with the software of GraphPad Prism 8 by fitting dose-response curves. Experiments were performed thrice with triplicate wells in each experiment.

**CETSA assay.** The MRSA strain was used for CETSA assay and the strain was cultured at 37 °C with TSB and incubated with DMSO or 43Hf for 2 h. After bacteria harvest, the cell pellets were resuspended in TE buffer (10 mM Tris, pH 8.0, 1 mM

EDTA) to approximately $4 \times 10^9$ CFU/mL. The lysostaphin (1 mg/mL) was added and the suspension was incubated at 37 °C for 30 min. After centrifugation, the supernatant was aliquoted to PCR tubes and heated at the appointed temperatures for 5 min. The tubes were placed at RT for another 3 min, then cooled on ice. The samples were centrifuged at 20,000 g for 20 min and the supernatant were subjected to western blot assay. The protein bands were detected by rabbit polyclonal anti-ClpP antibody.

**MRSA skin infection.** Animal studied were performed in accordance with the guidelines of the Care and Use of Laboratory Animals of Sichuan University. Five groups (n=5) of 6-8 weeks old Female BALB/c were used for the experiment. The fur on the back of the mice were shaved using a sterile razor and treated the shaved area with depilatory paste 1 day prior to inoculation. One group of mice (n=5) were treated with PBS as the control. Other groups of mice received a subcutaneous injection (50 μL) of $1.7 \times 10^9$ CFU/mL live MRSA ATCC 33591 to induce formation of abscess after 24 h. After injection for 6 h, the vehicle or compounds were injected into the shaved area of the skin where bacteria were injected. In the experiment, one group of mice was treated with the vehicle alone as the negative control and the other group of mice was treated with 40 μL vancomycin (3 mg/kg). Group 4 and 5 of mice was treated with 40 μL 43Hf (3 mg/kg and 1.5 mg/kg respectively). The dosage for each group were continued once daily for four days and the animal weights were measured every day. The mice were sacrificed after 12 h of the last dose and the infected skin was aseptically extracted and subsequently homogenized in 1 mL sterile saline. The

serially diluted homogenate was plate onto LB agar plates and incubated at 37 °C for at least 16 h. The bacterial titer was expressed as $\log_{10}$ CFU/abscess. The blood samples were collected on day 4 and day 14, then the collected samples were centrifuged at 3,500 rpm for 15 min for biochemistry analysis. P value was calculated by *t* tests using the software of GraphPad Prism 8 and a value of $P < 0.05$ was considered significant. The infected skin and major organs (heart, liver, spleen, lung and kidney) were harvested on day 4 and fixed with 4% paraformaldehyde. The tissues were stained with H & E and examined under an optical microscopy.

## Associated Content

### Supporting Information

Building blocks for the focused virtual library and the combinatorial synthesis; Validation of the multistep and micro-scale synthesis route; X-ray refinement statistics; additional figures and tables related biological studies; NMR spectra of final compounds and HPLC chromatogram of final compounds (PDF); Molecular formula strings (CSV).

### Accession Codes

Coordinates and structure factors for structures of bortezomib and 43Hf have been deposited in the Protein Data Bank with the accession code of 6L40 and 6L3X.

Authors will release the atomic coordinates and experimental data upon article publication.

## Author Information

### Corresponding Authors

***E-mail addresses: luo_youfu@scu.edu.cn, baorui@scu.edu.cn**

### Author Contributions

[#]Yuan Ju, Lihui He, Yuanzheng Zhou and Tao Yang contributed equally to this work.

### Funding Sources

The research was funded by the National Major Scientific and Technological Special Project for 'Significant New Drugs Development' #2019ZX09721001-001-001, the National Natural Science Foundation of China (#81973368, #81670008, #81871615), National Key Research and Development Plan (#SQ2016YFJC040104).

### Acknowledgements

We thank National Center for Protein Sciences Shanghai (NCPSS) beamline BL19U for beamtime allowance. We also thank the staffs of the Shanghai Synchrotron Radiation Facility (SSRF) beamline BL-17U and BL-18U, Shanghai, People's Republic of China, for assistance during data collection.

### Abbreviations Used

ClpP, caseinolytic protease P; Hla, α-hemolysis; agr, accessory gene regulator; DSC, differential scanning calorimetry; ITC, isothermal titration calorimetry; $K_d$, dissociation constant; MLN9708, ixazomib citrate; MLN2238, ixazomib; BTZ,

bortezomib; HPLC, high performance chromatography; UPLC-MS, Ultra performance liquid chromatography-mass spectrometer; SAR, structure-activity relationship; $K_i$, comparing inhibition constant; $K_{inact}$, enzyme inactivation rate; DSF, differential scanning fluorimetry; FITC-casein, fluorescein isothiocyanate-labeled casein; FXa, Factor Xa; MRSA, methicillin-resistant S. *aureus*; qPCR, quantitative polymerase chain reaction; CETSA, cellular thermal shift assay; Van, vancomycin; CREA, creatinine; UA, uric acid; BUN, blood urea nitrogen; LDH, lactate dehydrogenase; DBIL, direct bilirubin; AST, aspartate transaminase; ALB, albumin; TP, total protein; ALP, alkaline phosphatase; ALT, alanine transaminase; H&E, haematoxylin and eosin; MHB, Mueller-Hinton broth; CAMHB, cation-adjusted MHB; TSB, tryptone soy broth; Suc-LY-AMC, N-succinyl-Leu-Tyr-amido-4-methylcoumarin.

## References

(1) Frees, D.; Gerth, U.; Ingmer, H. Clp Chaperones and Proteases Are Central in Stress Survival, Virulence and Antibiotic Resistance of Staphylococcus Aureus. *Int. J. Med. Microbiol.* **2014**, *304* (2), 142–149.

(2) Raju, R. M.; Unnikrishnan, M.; Rubin, D. H. F.; Krishnamoorthy, V.; Kandror, O.; Akopian, T. N.; Goldberg, A. L.; Rubin, E. J. Mycobacterium Tuberculosis ClpP1 and ClpP2 Function Together in Protein Degradation and Are Required for Viability in Vitro and During Infection. *PLoS Pathog.* **2012**, *8* (2), e1002511.

(3) Frees, D.; Qazi, S. N. A.; Hill, P. J.; Ingmer, H. Alternative Roles of ClpX and ClpP in Staphylococcus Aureus Stress Tolerance and Virulence. *Mol. Microbiol.* **2003**, *48* (6), 1565–1578.

(4) Gaillot, O.; Pellegrini, E.; Bregenholt, S.; Nair, S.; Berche, P. The ClpP Serine Protease Is Essential for the Intracellular Parasitism and Virulence of Listeria Monocytogenes. *Mol. Microbiol.* **2002**, *35* (6), 1286–1294.

(5) Kwon, H. Y.; Ogunniyi, A. D.; Choi, M. H.; Pyo, S. N.; Rhee, D. K.; Paton, J. C. The ClpP Protease of Streptococcus Pneumoniae Modulates Virulence Gene Expression and Protects against Fatal Pneumococcal Challenge. *Infect. Immun.* **2004**, *72* (10), 5646–5653.

(6) Qiu, D.; Eisinger, V. M.; Head, N. E.; Pier, G. B.; Yu, H. D. ClpXP Proteases Positively Regulate Alginate Overexpression and Mucoid Conversion in Pseudomonas Aeruginosa. *Microbiology* **2008**, *154* (7), 2119–2130.

(7) Rasko, D. A.; Sperandio, V. Anti-Virulence Strategies to Combat Bacteria-Mediated Disease. *Nat. Rev. Drug Discov.* **2010**, *9* (2), 117–128.

(8) Haddad Kashani, H.; Schmelcher, M.; Sabzalipoor, H.; Seyed Hosseini, E.; Moniri, R. Recombinant Endolysins as Potential Therapeutics against Antibiotic-Resistant Staphylococcus Aureus : Current Status of Research and Novel Delivery Strategies. *Clin. Microbiol. Rev.* **2017**, *31* (1), e00071-17.

(9) Frees, D.; Sorensen, K.; Ingmer, H. Global Virulence Regulation in Staphylococcus Aureus: Pinpointing the Roles of ClpP and ClpX in the Sar/agr Regulatory Network. *Infect. Immun.* **2005**, *73* (12), 8100–8108.

(10) Weinandy, F.; Lorenz-Baath, K.; Korotkov, V. S.; Böttcher, T.; Sethi, S.; Chakraborty, T.; Sieber, S. A. A β-Lactone-Based Antivirulence Drug Ameliorates Staphylococcus Aureus Skin Infections in Mice. *ChemMedChem* **2014**, *9* (4), 710–713.

(11) Böttcher, T.; Sieber, S. A. β-Lactones as Specific Inhibitors of ClpP Attenuate the Production of Extracellular Virulence Factors of Staphylococcus Aureus. *J. Am. Chem. Soc.* **2008**, *130* (44), 14400–14401.

(12) Hackl, M. W.; Lakemeyer, M.; Dahmen, M.; Glaser, M.; Pahl, A.; Lorenz-Baath, K.; Menzel, T.; Sievers, S.; Böttcher, T.; Antes, I.; Waldmann, H.; Sieber, S. A. Phenyl Esters Are Potent Inhibitors of Caseinolytic Protease P and Reveal a Stereogenic Switch for Deoligomerization. *J. Am. Chem. Soc.* **2015**, *137* (26), 8475–8483.

(13) Pahl, A.; Lakemeyer, M.; Vielberg, M.-T.; Hackl, M. W.; Vomacka, J.; Korotkov, V. S.; Stein, M. L.; Fetzer, C.; Lorenz-Baath, K.; Richter, K.; Waldmann, H.; Groll, M.; Sieber, S. A. Reversible Inhibitors Arrest ClpP in a Defined Conformational State That Can Be Revoked by ClpX Association. *Angew. Chemie Int. Ed.* **2015**, *54* (52), 15892–15896.

(14) Moreira, W.; Ngan, G. J. Y.; Low, J. L.; Poulsen, A.; Chia, B. C. S.; Ang, M. J. Y.; Yap, A.; Fulwood, J.; Lakshmanan, U.; Lim, J.; Khoo, A. Y.; Flotow, H.; Hill, J.; Raju, R. M.; Rubin, E. J.; Dick, T. Target Mechanism-Based Whole-Cell Screening Identifies Bortezomib as an Inhibitor of Caseinolytic Protease in Mycobacteria. *MBio* **2015**, *6* (3), e00253-15.

(15) Akopian, T.; Kandror, O.; Tsu, C.; Lai, J. H.; Wu, W.; Liu, Y.; Zhao, P.; Park, A.; Wolf, L.; Dick, L. R.; Rubin, E. J.; Bachovchin, W.; Goldberg, A. L. Cleavage Specificity of Mycobacterium Tuberculosis ClpP1P2 Protease and Identification of Novel Peptide Substrates and Boronate Inhibitors with Anti-Bacterial Activity. *J. Biol. Chem.* **2015**, *290* (17), 11008–11020.

(16) Tan, J.; Grouleff, J. J.; Jitkova, Y.; Diaz, D. B.; Griffith, E. C.; Shao, W.; Bogdanchikova, A. F.; Poda, G.; Schimmer, A. D.; Lee, R. E.; Yudin, A. K. De Novo Design of Boron-Based Peptidomimetics as Potent Inhibitors of Human ClpP in the Presence of Human ClpX. *J. Med. Chem.* **2019**, *62* (13), 6377–6390.

(17) Mundra, S.; Thakur, V.; Bello, A. M.; Rathore, S.; Asad, M.; Wei, L.; Yang, J.; Chakka, S. K.; Mahesh, R.; Malhotra, P.; Mohmmed, A.; Kotra, L. P. A Novel Class of Plasmodial ClpP Protease Inhibitors as Potential Antimalarial Agents. *Bioorg. Med. Chem.* **2017**, *25* (20), 5662–5677.

(18) Szyk, A.; Maurizi, M. R. Crystal Structure at 1.9A of E. Coli ClpP with a Peptide Covalently Bound at the Active Site. *J. Struct. Biol.* **2006**, *156* (1), 165–174.

(19) Moreno-Cinos, C.; Sassetti, E.; Salado, I. G.; Witt, G.; Benramdane, S.; Reinhardt, L.; Cruz, C. D.; Joossens, J.; Van der Veken, P.; Brötz-Oesterhelt, H.; Tammela, P.; Winterhalter, M.; Gribbon, P.; Windshügel, B.; Augustyns, K. α-Amino Diphenyl Phosphonates as Novel Inhibitors of Escherichia Coli ClpP Protease. *J. Med. Chem.* **2019**, *62* (2), 774–797.

(20) Desai, B.; Dixon, K.; Farrant, E.; Feng, Q.; Gibson, K. R.; van Hoorn, W. P.; Mills, J.; Morgan, T.; Parry, D. M.; Ramjee, M. K.; Selway, C. N.; Tarver, G. J.; Whitlock, G.; Wright, A. G. Rapid Discovery of a Novel Series of Abl Kinase Inhibitors by Application of an Integrated Microfluidic Synthesis and Screening Platform. *J. Med. Chem.* **2013**, *56* (7), 3033–3047.

(21) Price, A. K.; MacConnell, A. B.; Paegel, B. M. hvSABR: Photochemical Dose-Response Bead Screening in Droplets. *Anal. Chem.* **2016**, *88* (5), 2904–2911.

(22) Usanov, D. L.; Chan, A. I.; Maianti, J. P.; Liu, D. R. Second-Generation DNA-Templated Macrocycle Libraries for the Discovery of Bioactive Small Molecules. *Nat. Chem.* **2018**, *10* (7), 704–714.

(23) Frei, P.; Hevey, R.; Ernst, B. Dynamic Combinatorial Chemistry: A New Methodology Comes of Age. *Chemistry* **2019**, *25* (1), 60–73.

(24) Gesmundo, N. J.; Sauvagnat, B.; Curran, P. J.; Richards, M. P.; Andrews, C. L.; Dandliker, P. J.; Cernak, T. Nanoscale Synthesis and Affinity Ranking. *Nature* **2018**, *557* (7704), 228–232.

(25) Bajorath, J. Integration of Virtual and High-Throughput Screening. *Nat. Rev. Drug Discov.* **2002**, *1* (11), 882–894.

(26) Kupperman, E.; Lee, E. C.; Cao, Y.; Bannerman, B.; Fitzgerald, M.; Berger, A.; Yu, J.; Yang, Y.; Hales, P.; Bruzzese, F.; Liu, J.; Blank, J.; Garcia, K.; Tsu, C.; Dick, L.; Fleming, P.; Yu, L.; Manfredi, M.; Rolfe, M.; Bolen, J. Evaluation of

the Proteasome Inhibitor MLN9708 in Preclinical Models of Human Cancer. *Cancer Res*. **2010**, *70* (5), 1970–1980.

(27) Smoum, R.; Rubinstein, A.; Dembitsky, V. M.; Srebnik, M. Boron Containing Compounds as Protease Inhibitors. *Chem. Rev*. **2012**, *112* (7), 4156–4220.

(28) Baker, S. J.; Tomsho, J. W.; Benkovic, S. J. Boron-Containing Inhibitors of Synthetases. *Chem. Soc. Rev*. **2011**, *40* (8), 4279–4285.

(29) Diaz, D. B.; Yudin, A. K. The Versatility of Boron in Biological Target Engagement. *Nat. Chem*. **2017**, *9* (8), 731–742.

(30) Vazquez-Rodriguez, S.; Wright, M.; Rogers, C. M.; Cribbs, A. P.; Velupillai, S.; Philpott, M.; Lee, H.; Dunford, J. E.; Huber, K. V. M.; Robers, M. B.; Vasta, J. D.; Thezenas M. L.; Bonham, S.; Kessler, B.; Bennett, J.; Fedorov, O.; Raynaud, F.; Donovan, A.; Blagg, J.; Bavetsias, V.; Oppermann, U.; Bountra, C.; Kawamura, A.; Brennan, P. E. Design, Synthesis and Characterization of Covalent KDM5 Inhibitors. *Angew. Chem. Int. Ed. Engl*. **2019**, *58* (2), 515–519.

(31) Krippendorff, B.-F.; Neuhaus, R.; Lienau, P.; Reichel, A.; Huisinga, W. Mechanism-Based Inhibition: Deriving K(I) and K(inact) Directly from Time-Dependent IC(50) Values. *J. Biomol. Screen*. **2009**, *14* (8), 913–923.

(32) Gersch, M.; Kolb, R.; Alte, F.; Groll, M.; Sieber, S. A. Disruption of Oligomerization and Dehydroalanine Formation as Mechanisms for ClpP Protease Inhibition. *J. Am. Chem. Soc*. **2014**, *136* (4), 1360–1366.

(33) Akçay, G.; Belmonte, M. A.; Aquila, B.; Chuaqui, C.; Hird, A. W.; Lamb, M. L.; Rawlins, P. B.; Su, N.; Tentarelli, S.; Grimster, N. P.; Su, Q. Inhibition of Mcl-1

through Covalent Modification of a Noncatalytic Lysine Side Chain. *Nat. Chem. Biol.* **2016**, *12* (11), 931–936.

(34) Zhou, Z.; Chen, X.; Fu, Y.; Zhang, Y.; Dai, S.; Li, J.; Chen, L.; Xu, G.; Chen, Z.; Chen, Y. Characterization of FGF401 as a Reversible Covalent Inhibitor of Fibroblast Growth Factor Receptor 4. *Chem. Commun.* **2019**, *55* (42), 5890–5893.

(35) Gronauer, T. F.; Mandl, M. M.; Lakemeyer, M.; Hackl, M. W.; Meßner, M.; Korotkov, V. S.; Pachmayr, J.; Sieber, S. A. Design and Synthesis of Tailored Human Caseinolytic Protease P Inhibitors. *Chem. Commun.* **2018**, *54* (70), 9833–9836.

(36) Hall, B. M.; Breidenstein, E. B. M.; de la Fuente-Núñez, C.; Reffuveille, F.; Mawla, G. D.; Hancock, R. E. W.; Baker, T. A. Two Isoforms of Clp Peptidase in Pseudomonas Aeruginosa Control Distinct Aspects of Cellular Physiology. *J. Bacteriol.* **2017**, *199* (3), e00568-16.

(37) Cezairliyan, B. O.; Sauer, R. T. Control of Pseudomonas Aeruginosa AlgW Protease Cleavage of MucA by Peptide Signals and MucB. *Mol. Microbiol.* **2009**, *72* (2), 368–379.

(38) Maignan, S.; Guilloteau, J. P.; Pouzieux, S.; Choi-Sledeski, Y. M.; Becker, M. R.; Klein, S. I.; Ewing, W. R.; Pauls, H. W.; Spada, A. P.; Mikol, V. Crystal Structures of Human Factor Xa Complexed with Potent Inhibitors. *J. Med. Chem.* **2000**, *43* (17), 3226–3232.

(39) Ni, T.; Ye, F.; Liu, X.; Zhang, J.; Liu, H.; Li, J.; Zhang, Y.; Sun, Y.; Wang, M.; Luo, C.; Jiang, H.; Lan, L.; Gan, J.; Zhang, A.; Zhou, H.; Yang, C. G. Characterization of Gain-of-Function Mutant Provides New Insights into ClpP Structure. *ACS Chem. Biol.* **2016**, *11* (7), 1964–1972.

(40) Otwinowski, Z.; Minor, W. Processing of X-Ray Diffraction Data Collected in Oscillation Mode. *Methods in Enzymology* **1997**, 276, 307–326.

(41) Geiger, S. R.; Böttcher, T.; Sieber, S. A.; Cramer, P. A Conformational Switch Underlies ClpP Protease Function. *Angew. Chemie Int. Ed.* **2011**, *50* (25), 5749–5752.

(42) Ye, F.; Zhang, J.; Liu, H.; Hilgenfeld, R.; Zhang, R.; Kong, X.; Li, L.; Lu, J.; Zhang, X.; Li, D.; Jiang, H.; Yang, C. G.; Luo, C. Helix Unfolding/refolding Characterizes the Functional Dynamics of Staphylococcus Aureus Clp Protease. *J. Biol. Chem.* **2013**, *288* (24), 17643–17653.

(43) Balogh, D.; Dahmen, M.; Stahl, M.; Poreba, M.; Gersch, M.; Drag, M.; Sieber, S. A. Insights into ClpXP Proteolysis: Heterooligomerization and Partial Deactivation Enhance Chaperone Affinity and Substrate Turnover in Listeria Monocytogenes. *Chem. Sci.* **2017**, *8* (2), 1592–1600.

(44) Zeiler, E.; List, A.; Alte, F.; Gersch, M.; Wachtel, R.; Poreba, M.; Drag, M.; Groll, M.; Sieber, S. A. Structural and Functional Insights into Caseinolytic Proteases Reveal an Unprecedented Regulation Principle of Their Catalytic Triad. *Proc. Natl. Acad. Sci. U. S. A.* **2013**, *110* (28), 11302–11307.

(45) Frees, D.; Andersen, J. H.; Hemmingsen, L.; Koskenniemi, K.; Bæk, K. T.; Muhammed, M. K.; Gudeta, D. D.; Nyman, T. A.; Sukura, A.; Varmanen, P.; Savijoki, K. New Insights into Staphylococcus Aureus Stress Tolerance and Virulence Regulation from an Analysis of the Role of the ClpP Protease in the Strains Newman, COL, and SA564. *J. Proteome Res.* **2012**, *11* (1), 95–108.

(46) Gao, P.; Ho, P. L.; Yan, B.; Sze, K. H.; Davies, J.; Kao, R. Y. T. Suppression of Staphylococcus Aureus Virulence by a Small-Molecule Compound. *Proc. Natl. Acad. Sci. U. S. A.* **2018**, *115* (31), 8003–8008.

(47) Jafari, R.; Almqvist, H.; Axelsson, H.; Ignatushchenko, M.; Lundbäck, T.; Nordlund, P.; Molina, D. M. The Cellular Thermal Shift Assay for Evaluating Drug Target Interactions in Cells. *Nat. Protoc.* **2014**, *9* (9), 2100–2122.

(48) Farver, C. F.; Zander, D. S. Molecular Basis of Pulmonary Disease. In *Molecular Pathology*; Elsevier, 2009; pp 305–364.

(49) Böttcher, T.; Sieber, S. A. Structurally Refined β-Lactones as Potent Inhibitors of Devastating Bacterial Virulence Factors. *ChemBioChem* **2009**, *10* (4), 663–666.

(50) Gersch, M.; Famulla, K.; Dahmen, M.; Göbl, C.; Malik, I.; Richter, K.; Korotkov, V. S.; Sass, P.; Rübsamen-Schaeff, H.; Madl, T.; Brötz-Oesterhelt, H.; Sieber, S. A. AAA+ Chaperones and Acyldepsipeptides Activate the ClpP Protease via Conformational Control. *Nat. Commun.* **2015**, *6*, 6320.

(51) Fedorov, O.; Niesen, F. H.; Knapp, S. Kinase Inhibitor Selectivity Profiling Using Differential Scanning Fluorimetry. *Methods Mol. Biol.* **2012**, 795, 109–118.

(52) Adams, P. D.; Afonine, P. V.; Bunkóczi, G.; Chen, V. B.; Davis, I. W.; Echols, N.; Headd, J. J.; Hung, L. W.; Kapral, G. J.; Grosse-Kunstleve, R. W.; McCoy, A. J.; Moriarty, N. W.; Oeffner, R.; Read, R. J.; Richardson, D. C.; Richardson, J. S.; Terwilliger, T. C.; Zwart, P. H. PHENIX: A Comprehensive Python-Based System for Macromolecular Structure Solution. *Acta Crystallogr. Sect. D Biol. Crystallogr.* **2010**, *66* (2), 213–221.

(53) Emsley, P.; Cowtan, K. Coot: Model-Building Tools for Molecular Graphics. *Acta Crystallogr. Sect. D Biol. Crystallogr.* **2004**, *60* (12 I), 2126–2132.

## Table of Contents Graphic